INTERNATIONAL JOURNAL FOR NUMERICAL METHODS IN ENGINEERING
*Int. J. Numer. Meth. Engng* 2002; **55**:1255–1284 (DOI: 10.1002/nme.619)

# Improvements and algorithmical considerations on a recent three-dimensional model describing stress-induced solid phase transformations

Ferdinando Auricchio[1,2,*,†] and Lorenza Petrini[1]

[1]*Dipartimento di Meccanica Strutturale, Università di Pavia, Via Ferrata 1, 27100 Pavia, Italy*
[2]*Istituto di Matematica Applicata e Tecnologie Informatiche, CNR, Via Ferrata 1, 27100 Pavia, Italy*

SUMMARY

During mechanical loading–unloading cycles shape-memory alloys (SMA) are able to undergo large deformations without showing residual strains (*pseudoelasticity*) or recovering them through thermal cycles (*shape memory effect*). Motivated by stress-induced solid phase transformations, these unique behaviours induce the SMA exploitation in innovative and commercially valuable applications, stimulating, consequently, the interest in the development of constitutive models. Also if many models are now available in the literature, effective three-dimensional proposals are still few and limited in several aspects.

In this paper, a three-dimensional thermomechanical model recently proposed by Souza *et al.* (*European Journal of Mechanics–A/Solids*, 1998; **17**:789–806.) is taken into consideration; such a model is of particular interest for its effectiveness and flexibility, but it also shows some limitations and missing links in the algorithmical counterparts.

This work discusses some improvements to the original model as well as the development and the implementation of a robust integration algorithm to be adopted in a numerical scheme, such as a finite-element framework. Copyright © 2002 John Wiley & Sons, Ltd.

KEY WORDS: shape memory alloys; solid phase transformation; 3D constitutive model; numerical implementation; return map; integration algorithm

## 1. INTRODUCTION

The good performances of *shape-memory alloys* (SMA) in applications relative to different fields (such as aeronautical, biomedical, structural engineering) is a consequence of the fact that the material may in general present two different crystallographic structures, one

*Correspondence to: Ferdinando Auricchio, Dipartimento di Meccanica Strutturale, Università di Pavia, Via Ferrata 1, 27100 Pavia, Italy
†E-mail: auricchio@unipv.it

Contract/grant sponsor: Italian National Center of Research

*Received 3 September 2001*
*Revised 5 June 2002*
*Accepted 5 June 2002*

characterized by a more ordered unit cell and indicated in the following as *austenite* (A), the other characterized by a less ordered unit cell and indicated in the following as *martensite* (M). Moreover, the martensite may have a global structure where the unit cells have a variable orientation minimizing the misfit with the surrounding material, or a global structure where the unit cells follow a preferred orientation given by an external field such as a stress; in the former case we talk of *twinned or multiple-variant martensite* (MV), in the latter case of *detwinned or single-variant martensite* (SV).

From a micro-mechanical point of view, the presence of two different crystallographic structures is the base for a reversible solid–solid phase transformation between the austenite and the martensite. The phase transformation is in general function of temperature and stress. In particular, for the case of a stress-free material, we may distinguish two reference temperatures, $A_f$ and $M_f$, with $A_f > M_f$, such that: the austenite is the only phase stable at temperatures above $A_f$; the martensite is the only phase stable at temperatures below $M_f$; an austenite–martensite mixture is possible in the temperature interval between $A_f$ and $M_f$. In general, both $A_f$ and $M_f$ depend on the material composition as well as on the thermomechanical treatment. For the case of a stressed material, a similar situation occurs, with the difference that the reference temperatures are monotonic (approximately linear) function of the loading level.

From a macro-mechanical point of view, the reversible martensitic phase transformation results in two unique effects, the *pseudoelasticity* (PE) and the *shape memory effect* (SME) [1, 2]. At temperatures above $A_f$, if loaded the material shows non-linear large deformations, which are recovered during the unloading, describing an hysteretic loop in terms of stress and strain (pseudoelasticity). This response can be explained noting that the load induces a transformation from austenite to single-variant martensite; however, since the austenite is the only phase stable above $A_f$, the reverse transformation occurs during the unloading. At temperatures below $A_f$, if loaded the material shows non-linear large deformations, which are partially retained during the unloading; however, this residual strain can be recovered heating the material above $A_f$ (shape memory effect). This response can be explained noting that the load induces a transformation from austenite or multiple-variant martensite to single-variant martensite. However, since the martensite is unstable above $A_f$, heating the material a transformation from martensite to austenite occurs and the material recovers the initial shape; moreover, such a shape is retained also during the cooling at the initial temperature [3].

The more and more frequent use of these unusual effects in commercially valuable applications have stimulated a vivid interest in the development of accurate constitutive models, able to catch the basic material response, and in their algorithmic counterparts [4, 5]. However, while many 1D models are available in the literature [6–9], effective proposals in 3D framework are still few and limited in several aspects: in particular, their numerical implementation and exploitation in numerical codes do not seem easy to achieve and sufficiently robust [10–16].

Accordingly, we focus on a three-dimensional thermomechanical model recently proposed by Souza *et al.* [17] for stress-induced solid phase transformations. Cast within the framework of classical irreversible thermodynamics, the model is able to reproduce all the main features relative to shape-memory materials in a 3D setting. In particular, Souza *et al.* consider some simple one-dimensional problems as well as a more complex three-dimensional non-proportional problem, showing a good performance of the model in comparison with experimental results.

 

However, a careful reading of the cited work on one hand shows some interesting features of the model, in particular the effectiveness and the flexibility of the adopted framework, as well as some limitations, mainly relative to a symmetric tension–compression material response and to the assumption of a small-deformation regime. On the other hand, it highlights how the proposed return map integration algorithm is only partially developed: some missing links make the time-discrete solution scheme not suitable for an effective numerical implementation.

Accordingly, in the present paper we propose some improvements to the original model, focusing on the development of a robust integration algorithm to be adopted in a numerical scheme, such as a finite-element framework. We also investigate a possible model extension to describe unsymmetrical behaviours in tension and compression.

The paper is organized as follows. Section 2 reviews the original model as proposed by Souza *et al.*, both in the time-continuous and the time-discrete frame, together with some comments on the relative merits and shortcomings. Section 3 describes in details a modified integration algorithm, which is tested in Section 4 for the case of several one-dimensional and multi-dimensional problems. Comments and suggestions for future developments are reported in Section 5; finally, in Appendix A.1 possible model extension is discussed to catch the unsymmetrical behaviour of the material in tension and compression.

## 2. ORIGINAL MODEL FOR STRESS-INDUCED SOLID PHASE TRANSFORMATION

The model proposed by Souza *et al.* is developed within the theory of irreversible thermodynamics in the realm of a small-deformation regime [18, 19]. Accordingly, at each instant the thermodynamical state of an homogenized volume element is described by a set of external (controllable) and internal variables. Moreover, given proper potentials and following classical arguments, it is possible to compute the quantities thermodynamically conjugate to both the external and the internal variables.

The goal of this section is to briefly review the *original model* [17] and to present comments highlighting features and limitations of the model.

Before proceeding, we find convenient to split the strain, $\boldsymbol{\varepsilon}$, and the stress, $\boldsymbol{\sigma}$, as follows:

$$\boldsymbol{\varepsilon} = \mathbf{e} + \mathbf{1}\frac{\theta}{3} \tag{1}$$

$$\boldsymbol{\sigma} = \mathbf{s} + \mathbf{1}p \tag{2}$$

where: $\mathbf{e}$ is the deviatoric strain; $\theta = \boldsymbol{\varepsilon} : \mathbf{1}$ is the volumetric strain; $\mathbf{s}$ is the deviatoric stress; $p = \boldsymbol{\sigma} : \mathbf{1}/3$ is the volumetric stress, in general indicated as pressure.

### 2.1. Time-continuous frame

Souza *et al.* choose the strain, $\boldsymbol{\varepsilon}$, split in its volumetric and deviatoric components, and the absolute temperature, $T$, as control variables and a second-order tensor, $\mathbf{e}^{\mathrm{tr}}$, indicated as *transformation strain*, as internal variable. Assumed to be traceless, $\mathbf{e}^{\mathrm{tr}}$ is a measure of the strain associated to the phase transformation and, in particular, to the conversion from austenite or multiple-variant martensite to the single-variant martensite. Accordingly, the norm of $\mathbf{e}^{\mathrm{tr}}$

 

should be bounded between zero—for the case of a material without oriented martensite—and a maximum value $\varepsilon_L$—for the case in which the material is fully transformed in single-variant oriented martensite.

Henceforth, Souza *et al.* set the free-energy equal to:

$$\psi(\theta, \mathbf{e}, T, \mathbf{e}^{\mathrm{tr}}) = \tfrac{1}{2} K\theta^2 + G\|\mathbf{e} - \mathbf{e}^{\mathrm{tr}}\|^2 + \tau_M(T)\|\mathbf{e}^{\mathrm{tr}}\| + \frac{h}{2}\|\mathbf{e}^{\mathrm{tr}}\|^2 + \mathscr{I}_{\varepsilon_L}(\mathbf{e}^{\mathrm{tr}}) \tag{3}$$

where: $K$ and $G$ are the bulk and the shear moduli; $\|\cdot\|$ is the Euclidean norm; $\tau_M$ is a positive and monotonically increasing function of the temperature, defined as $\langle\beta(T - T_0)\rangle^+$, with $\langle\bullet\rangle^+$ the positive part of the argument, $\beta$ a material parameter, $T$ the room temperature and $T_0$ the temperature below which no twinned martensite is observed; $h$ is a material parameter related to the hardening of the material during the phase transformation. Finally, $\mathscr{I}_{\varepsilon_L}(\mathbf{e}^{\mathrm{tr}})$ is an indicator function introduced to satisfy the constraint on the transformation strain norm and defined as:

$$\mathscr{I}_{\varepsilon_L}(\mathbf{e}^{\mathrm{tr}}) = \begin{cases} 0 & \text{if } \|\mathbf{e}^{\mathrm{tr}}\| \leqslant \varepsilon_L \\ +\infty & \text{otherwise} \end{cases} \tag{4}$$

Following classical arguments, it is possible to compute the quantities thermodynamically conjugate to the volumetric and the deviatoric components of the strain, $\theta$ and $\mathbf{e}$, and to the transformation strain, $\mathbf{e}^{\mathrm{tr}}$. In particular, we have:

$$p = \frac{\partial\psi}{\partial\theta} = K\theta \tag{5}$$

$$\mathbf{s} = \frac{\partial\psi}{\partial\mathbf{e}} = 2G(\mathbf{e} - \mathbf{e}^{\mathrm{tr}}) \tag{6}$$

$$\mathbf{X} = -\frac{\partial\psi}{\partial\mathbf{e}^{\mathrm{tr}}} = \mathbf{s} - \boldsymbol{\alpha} \tag{7}$$

with $\mathbf{X}$ indicated in the following as *transformation stress* where:

$$\boldsymbol{\alpha} = [\tau_M(T) + h\|\mathbf{e}^{\mathrm{tr}}\| + \gamma]\frac{\mathbf{e}^{\mathrm{tr}}}{\|\mathbf{e}^{\mathrm{tr}}\|} \tag{8}$$

with $\gamma$ defined as:

$$\begin{cases} \gamma = 0 & \text{if } 0 < \|\mathbf{e}^{\mathrm{tr}}\| < \varepsilon_L \\ \gamma \geqslant 0 & \text{if } \|\mathbf{e}^{\mathrm{tr}}\| = \varepsilon_L \end{cases} \tag{9}$$

It is interesting to observe that the quantity $\boldsymbol{\alpha}$ in Equation (7) plays a role similar to the so-called *back-stress* in classical plasticity and, accordingly, $\mathbf{X}$ can be identified as a *relative stress*. Moreover, we note that $\boldsymbol{\alpha}$ is defined only for the case $\|\mathbf{e}^{\mathrm{tr}}\| > 0$.

Thereupon, the introduction of a dissipation pseudopotential in the form:

$$\phi(\dot{\mathbf{e}}^{\mathrm{tr}}) = R\|\dot{\mathbf{e}}^{\mathrm{tr}}\| \tag{10}$$

 

with $R$ the elastic domain radius, combined with a complementary evolution law in the form:

$$\mathbf{X} \in \partial\phi(\dot{\mathbf{e}}^{\mathrm{tr}}) \tag{11}$$

returns the following evolutionary equations for the internal variable $\mathbf{e}^{\mathrm{tr}}$:

$$\begin{cases} \dot{\mathbf{e}}^{\mathrm{tr}} = \dot{\zeta}\,\dfrac{\mathbf{X}}{\|\mathbf{X}\|} & \text{(12a)} \\ F(\mathbf{X}) = \|\mathbf{X}\| - R \leqslant 0 & \text{(12b)} \\ \dot{\zeta} \geqslant 0 & \text{(12c)} \\ \dot{\zeta} F(\mathbf{X}) = 0 & \text{(12d)} \end{cases}$$

where Equation (12a) is the flow rule, Equation (12b) defines the limit function $F$ in terms of the relative stress $\mathbf{X}$, Equations (12c)–(12d) are the classical Kuhn–Tucker conditions, which reduce the problem to a constrained optimization problem.

As highlighted in the original work, requiring the dissipation pseudopotential to be convex and positive and to have a null value at the origin ensures the thermodynamical consistency of the model, i.e. a non-negative value for the mechanical dissipation. Finally, after several argumentations on the evolution laws and on the nucleation criteria, it is possible to conclude that material can be either in an *elastic state*, in an *evolving phase transformation state*, or in a *saturated phase transformation state*. The proper material state is detected by the conditions presented in Table I and each material state is associated to the evolution equations presented in Table II.

*Comments on features and limits of the time-continuous frame*: From the previous brief review and keeping in mind Tables I and II, we may comment on some features and limits of the model, in part also explaining its ability to describe SMA characteristic behaviours in a 3D framework.

In particular, the following features of the model can be observed.

- The state and the branch detection are related to the norm of the transformation strain $\|\mathbf{e}^{\mathrm{tr}}\|$.
- All the phase transformations ($A \leftrightarrow SV$, $MV \rightarrow SV$) are described by a single limit function $F$.

  Defined in terms of the relative stress $\mathbf{X} = \mathbf{s} - \boldsymbol{\alpha}$, the limit function $F$ defines in the deviatoric space the region of admissible states ($F \leqslant 0$), distinguishing at the same time states for which phase transformations are not possible ($F < 0 \Rightarrow$ elastic domain) and states for which phase transformations may be possible ($F = 0$).

  In particular, the region of admissible states has a constant radius, $R$, and a moving centre, $\boldsymbol{\alpha}$, the latter depending on the temperature—through the function $\tau_M$—and on the phase transformation itself—through the material parameter $h$. Accordingly, during the phase transformation, $\boldsymbol{\alpha}$ increases proportionally to $\|\mathbf{e}^{\mathrm{tr}}\|$, moving the limit surface in the $\mathbf{e}^{\mathrm{tr}}$ direction.
- Since all the phase transformations are described by a single limit function $F$, the differences between SME and PE are caught through the dependency of the parameter $\tau_M$ on the temperature.

 

Table I. Original time-continuous frame: detection of the material state and of the evolution branch.

State and Branch Detection

$$
\begin{aligned}
&\text{if } (\|\mathbf{e}^{\mathrm{tr}}\| = 0) \text{ then}\\
&\quad \left\{ \begin{array}{l} \text{compute: } F = \|\mathbf{s}\| - [\tau_M(T) + R] \qquad (42)\\ \text{check } F: \left\{ \begin{array}{ll} \text{if } (F<0) \text{ then} & \textbf{elastic state}\\ \text{else} & \\ \quad \mathbf{X} = R\dfrac{\mathbf{s}}{\|\mathbf{s}\|} & \textbf{evolv. p.t.}\\ \text{end if} & \end{array} \right. \end{array} \right.\\
&\text{else if } (\|\mathbf{e}^{\mathrm{tr}}\| < \varepsilon_L) \text{ then}\\
&\quad \left\{ \begin{array}{l} \text{compute: } \left\{ \begin{array}{l} \boldsymbol{\alpha} = [\tau_M(T) + h\|\mathbf{e}^{\mathrm{tr}}\|]\dfrac{\mathbf{e}^{\mathrm{tr}}}{\|\mathbf{e}^{\mathrm{tr}}\|}\\ \mathbf{X} = \mathbf{s} - \boldsymbol{\alpha}\\ F = \|\mathbf{X}\| - R \end{array} \right. \qquad (43)\\ \text{check } F: \left\{ \begin{array}{ll} \text{if } (F<0) \text{ then} & \textbf{elastic state}\\ \text{else} & \textbf{evolv. p.t.}\\ \text{end if} & \end{array} \right. \end{array} \right.\\
&\text{else if } (\|\mathbf{e}^{\mathrm{tr}}\| = \varepsilon_L) \text{ then}\\
&\quad \left\{ \begin{array}{l} \text{compute: } \left\{ \begin{array}{l} \boldsymbol{\alpha} = [\tau_M(T) + h\|\mathbf{e}^{\mathrm{tr}}\| + \gamma]\dfrac{\mathbf{e}^{\mathrm{tr}}}{\|\mathbf{e}^{\mathrm{tr}}\|}\\ \gamma \geqslant 0\\ \mathbf{X} = \mathbf{s} - \boldsymbol{\alpha}\\ F = \|\mathbf{X}\| - R \end{array} \right. \qquad (44)\\ \text{check } F: \left\{ \begin{array}{ll} \text{if } (F<0) \text{ then} & \textbf{elastic state}\\ \text{else} & \textbf{satur. p.t.}\\ \text{end if} & \end{array} \right. \end{array} \right.\\
&\text{end if}
\end{aligned}
$$

To appreciate this aspects, assume the occurrence of a forward transformation during loading; then, during unloading, if the temperature is below $M_f$, only the elastic deformation can be recovered and residual strains are present at zero stress (SME), while if the temperature is above $A_f$ the material is able to undergo a reverse transformation strain and to recover the original shape (PE).

This aspect can be further elaborated considering a uni-axial tensile test during unloading phase, assuming for simplicity $h = 0$ and recalling that the phase transformation is associated to the conditions $F = 0$. Indicating with $s$ and $e$ the uni-axial (scalar) deviatoric stress and strain components and with $\alpha$ the uni-axial (scalar) back stress component,

 

Table II. Original time-continuous frame: evolution laws in the different branches.

| Branch Solution |
|---|
| if (elastic state) then |
| $\dot{\mathbf{e}}^{\mathrm{tr}} = \mathbf{0}$ |
| else if (evolving phase transformation) then |
| $\dot{\mathbf{e}}^{\mathrm{tr}} = \dot{\zeta}\,\dfrac{\mathbf{X}}{\|\mathbf{X}\|}$ with $\dot{\zeta} > 0,\ \dot{\zeta} F = 0$ |
| else if (saturated phase transformation) then |
| $\dot{\mathbf{e}}^{\mathrm{tr}} = \dot{\zeta}\,\dfrac{\mathbf{X}}{\|\mathbf{X}\|}$ with $\begin{cases} \dot{\zeta} > 0, \dot{\zeta} F = 0 \\ \dot{\mathbf{e}}^{\mathrm{tr}} \cdot \mathbf{e}^{\mathrm{tr}} = 0 \end{cases}$ |
| end if |

the uni-axial unloading condition implies: $s > 0,\ \dot{s} < 0$. Moreover, we assume that the position $s < \alpha$ (i.e. $X = s - \alpha < 0$) is reached during unloading and we recall that it is $\alpha = \tau_M$ (Equation (8)) in uni-axial case. Hence, the condition for the activation of the reverse transformation (i.e. to have PE) becomes:

$$F = |s - \alpha| - R = -s + \alpha - R = -s + \tau_M - R = 0 \tag{13}$$

Equation (13) is satisfied only if $s = \tau_M - R$.

Since we assume $s > 0$, the reverse transformation strain can take place only if $\tau_M > R$ and, recalling the definition of $\tau_M$, only if $T > \bar{T} = R/\beta + T_0$. Finally, if we assume $T_0 = M_f$ and $\bar{T} = A_f$, Equations (6)–(12) are able to simulate all the possible SMA behaviours: in particular, SME takes place if $T \leqslant T_0$, PE takes place if $T \geqslant \bar{T}$ and a mix of the two behaviours takes place if $T_0 < T < \bar{T}$.

- The model is able to describe the SV martensite reorientation. This ability is true, in particular, for the case of a fully saturated material ($\|\mathbf{e}^{\mathrm{tr}}\| = \varepsilon_L$), when the product phase can still experience strain changes due to the variant reorientation ($\overline{\|\dot{\mathbf{e}}^{\mathrm{tr}}\|} = 0$ and $\dot{\mathbf{e}}^{\mathrm{tr}} \neq 0$).

  The model takes into account these behaviours through the tensorial nature of the internal variable $\mathbf{e}^{\mathrm{tr}}$, which naturally implies the concept of variant orientation, and through the introduction of the internal variable $\gamma$ in the back stress definition (Equation (8)). Indeed, the scalar $\gamma$ measures the limit surface movement in the $\mathbf{e}^{\mathrm{tr}}$ direction during the saturated phase, guaranteeing the satisfaction of the condition $F = 0$. In particular, it varies linearly when the product phase undergoes elastic deformation, non-linearly when reorientation takes place.

Moreover, some limits of the model are evident.

- The austenite and the martensite have the same elastic modulus.
- The phase transformations are described through a Von Mises-type function, predicting a symmetric behaviour in tension and compression, in contrast with experimental evidences [20–23].
- The transformation stress $\mathbf{X}$, and consequently $F$, are *undetermined* [5] for the case $\|\mathbf{e}^{\mathrm{tr}}\| = 0$ (Equations (7) and (8)). This aspect is the source of problems in detecting

 

the phase transformation activation for a material completely in the parent phase. To overcome this limit, Souza *et al.* introduce some considerations on the relation between $\mathbf{s}$ and $\mathbf{X}$, proving that, when $\|\mathbf{e}^{\mathrm{tr}}\| \to 0$:

$$\frac{\mathbf{s}-\mathbf{X}}{\|\mathbf{s}-\mathbf{X}\|} \approx \frac{\mathbf{X}}{\|\mathbf{X}\|} \approx \frac{\mathbf{s}}{\|\mathbf{s}\|} \tag{14}$$

Accordingly, for the product phase nucleation the following conditions hold:

$$\begin{cases} \|\mathbf{s}\| = \tau_M(T) + R \\ \mathbf{X} = R\,\dfrac{\mathbf{s}}{\|\mathbf{s}\|} \end{cases} \tag{15}$$

and the limit function $F$ reduces as follows:

$$F = \|\mathbf{s}\| - (\tau_M(T) + R) \tag{16}$$

### 2.2. Time-discrete frame and solution algorithm

From a computational standpoint the non-linear material behaviour is often treated as an *implicit time-discrete strain-driven* problem. Accordingly, a time-discrete counterpart of the constitutive model is first introduced, integrating the model rate equations over a time interval $[t_n, t_{n+1}]$ using an implicit backward Euler scheme. Afterwards, assuming to know the solution at time $t_n$ as well as the strain $\boldsymbol{\varepsilon}$ at time $t_{n+1}$, the stress history is computed from the strain history by means of a procedure known as *return-map* [24–27].

For the model of the previous section, Souza *et al.* developed a time-discrete solution scheme along these lines and briefly reviewed in the following; to simplify the notation, we indicate with the subscript $n$ a quantity evaluated at time $t_n$, and with no subscript a quantity evaluated at time $t_{n+1}$.

Accordingly, the time-discrete counterpart of the constitutive model described in Section 2.1 is:

$$\begin{cases} \mathbf{s} = 2G(\mathbf{e} - \mathbf{e}^{\mathrm{tr}}) & \text{(17a)} \\ \mathbf{X} = \mathbf{s} - [\tau_M(T) + h\|\mathbf{e}^{\mathrm{tr}}\| + \gamma]\dfrac{\mathbf{e}^{\mathrm{tr}}}{\|\mathbf{e}^{\mathrm{tr}}\|} & \text{(17b)} \\ \gamma \geqslant 0 & \text{(17c)} \\ \mathbf{e}^{\mathrm{tr}} = \mathbf{e}^{\mathrm{tr}}_n + \Delta\zeta\,\dfrac{\mathbf{X}}{\|\mathbf{X}\|} & \text{(17d)} \\ \|\mathbf{e}^{\mathrm{tr}}\| \leqslant \varepsilon_L & \text{(17e)} \\ F(\mathbf{X}) = \|\mathbf{X}\| - R \leqslant 0 & \text{(17f)} \\ \Delta\zeta \geqslant 0 \;\; \Delta\zeta F(\mathbf{X}) = 0 & \text{(17g)} \end{cases}$$

where: $\Delta\zeta = (\zeta - \zeta_n)$ and where we omit to report the trivial elastic volumetric relation.

Souza *et al.* propose to solve such a time-discrete model through an elastic-predictor inelastic-corrector procedure. Reported in Table III, the procedure consists in computing

 

Table III. Original time-discrete frame: solution algorithm.

1. **Compute trial state**

$$\begin{cases} \mathbf{e}^{\mathrm{tr},TR} = \mathbf{e}_n^{\mathrm{tr}} \\ \mathbf{s}^{TR} = 2G(\mathbf{e} - \mathbf{e}^{\mathrm{tr},TR}) \\ \mathbf{n}^{TR} = \dfrac{\mathbf{e}^{\mathrm{tr},TR}}{\|\mathbf{e}^{\mathrm{tr},TR}\|} \end{cases}$$

2. **Check material state**
   See Table IV
3. **Update material state**
   See Table V

an elastic trial state and in evaluating the admissibility of such a state through $F^{TR}$, i.e. through the value of the limit function on the trial state. Then, if the trial state is admissible ($F^{TR} \leqslant 0$) the step is effectively elastic and it represents the solution; otherwise, if the trial state is non-admissible ($F^{TR} > 0$), the step is inelastic and a new solution has to be evaluated.

Regarding the detection of the trial state admissibility, it is interesting to emphasize how, as summarized in Table IV, the definition of the limit function $F^{TR}$ depends on the initial state condition; in particular:

- For the case $\|\mathbf{e}_n^{\mathrm{tr}}\| = 0$, $F^{TR}$ is defined through the considerations on the nucleation condition (Equation (16)), being $\mathbf{X}^{TR}$ undetermined.
- For the case $\|\mathbf{e}_n^{\mathrm{tr}}\| \neq 0$, $F^{TR}$ is defined by Equation (17f) with $\mathbf{X}^{TR}$ given by Equation (17b), being $\gamma = 0$ in the evolving phase transformation state and $\gamma \neq 0$ in the saturated phase transformation state.

In the case of an inelastic step, the updated state is evaluated solving the non-linear Equation (17) with an iterative method. In particular, as summarized in Table V, Souza *et al.* suggest the following procedure:

- Supposing ($0 < \|\mathbf{e}^{\mathrm{tr}}\| < \varepsilon_L$), assume $\gamma = 0$ and rewrite Equation (17) in the residual form:

$$\mathbf{R}^6(\mathbf{e}^{\mathrm{tr}}) = R\,\frac{\mathbf{e}^{\mathrm{tr}} - \mathbf{e}_n^{\mathrm{tr}}}{\|\mathbf{e}^{\mathrm{tr}} - \mathbf{e}_n^{\mathrm{tr}}\|} - 2G(\mathbf{e} - \mathbf{e}^{\mathrm{tr}}) + [\tau_M(T) + h\|\mathbf{e}^{\mathrm{tr}}\|]\frac{\mathbf{e}^{\mathrm{tr}}}{\|\mathbf{e}^{\mathrm{tr}}\|} = \mathbf{0} \tag{18}$$

  Then, the new value of $\mathbf{e}^{\mathrm{tr}}$ is evaluated solving these six scalar non-linear equations with a Newton–Raphson method.
- If the above solution is non admissible ($\|\mathbf{e}^{\mathrm{tr}}\| > \varepsilon_L$), assume $\gamma > 0$ and rewrite Equation (17) in the residual form:

$$\mathbf{R}^7(\mathbf{e}^{\mathrm{tr}}, \gamma) = \begin{cases} R\,\dfrac{\mathbf{e}^{\mathrm{tr}} - \mathbf{e}_n^{\mathrm{tr}}}{\|\mathbf{e}^{\mathrm{tr}} - \mathbf{e}_n^{\mathrm{tr}}\|} - 2G(\mathbf{e} - \mathbf{e}^{\mathrm{tr}}) + [\tau_M(T) + h\|\mathbf{e}^{\mathrm{tr}}\| + \gamma]\dfrac{\mathbf{e}^{\mathrm{tr}}}{\|\mathbf{e}^{\mathrm{tr}}\|} = \mathbf{0} \\ \|\mathbf{e}^{\mathrm{tr}}\| - \varepsilon_L = 0 \end{cases} \tag{19}$$

  Then, the new values of $\mathbf{e}^{\mathrm{tr}}$ and $\gamma$ can be evaluated solving these seven scalar non-linear equations with a Newton–Raphson method.

 

Table IV. Original time-discrete frame: detection of the material state and of the evolution branch.

State and Branch Detection

if $(\|\mathbf{e}_n^{\mathrm{tr}}\| = 0)$ then

$$\begin{cases} \text{compute:} & F^{TR} = \|\mathbf{s}^{TR}\| - [\tau_M(T) + R] \\ \text{check } F^{TR}\text{:} & \begin{cases} \text{if } (F^{TR} < 0) \text{ then} & \textbf{elastic step } (EL) \\ \text{else} & \\ \quad \mathbf{X}^{TR} = R\dfrac{\mathbf{s}^{TR}}{\|\mathbf{s}^{TR}\|} & \textbf{active p.t. } (PT_1) \\ \text{end if} & \end{cases} \end{cases} \tag{45}$$

else if $(\|\mathbf{e}_n^{\mathrm{tr}}\| < \varepsilon_L)$ then

$$\begin{cases} \text{compute:} & \begin{cases} \boldsymbol{\alpha}^{TR} = [\tau_M(T) + h\|\mathbf{e}^{\mathrm{tr},TR}\|]\mathbf{n}^{TR} \\ \mathbf{X}^{TR} = \mathbf{s}^{TR} - \boldsymbol{\alpha}^{TR} \\ F^{TR} = \|\mathbf{X}^{TR}\| - R \end{cases} \\ \text{check } F^{TR}\text{:} & \begin{cases} \text{if } (F^{TR} < 0) \text{ then} & \textbf{elastic step } (EL) \\ \text{else} & \textbf{active p.t. } (PT_1) \\ \text{end if} & \end{cases} \end{cases} \tag{46}$$

else if $(\|\mathbf{e}_n^{\mathrm{tr}}\| = \varepsilon_L)$ then

$$\begin{cases} \text{compute:} & \begin{cases} \boldsymbol{\alpha}^{TR} = [\tau_M(T) + h\|\mathbf{e}^{\mathrm{tr},TR}\| + \hat{\gamma}]\mathbf{n}^{TR} \\ \mathbf{X}^{TR} = \mathbf{s}^{TR} - \boldsymbol{\alpha}^{TR} \\ F^{TR} = \|\mathbf{X}^{TR}\| - R \end{cases} \\ \text{check } F^{TR}\text{:} & \begin{cases} \text{if } (F^{TR} < 0) \text{ then} & \textbf{elastic step } (EL) \\ \text{else} & \textbf{active p.t. } (PT_1) \\ \text{end if} & \end{cases} \end{cases} \tag{47}$$

end if

*Comments on limits of the time-discrete frame*: Souza *et al.* do not detail the proposed algorithm as deeply as required by an effective numerical implementation, neglecting also to discuss the algorithmically consistent tangent matrix. In particular, a review of the proposed approach points out mainly two missing aspects, relative respectively to the definition of the transformation stress $\mathbf{X}$ and to the method for the solution of the non-linear problem.

- *Definition of* $\mathbf{X}$: Besides the problematics associated with the non-definition of $\mathbf{X}$ for the case $\|\mathbf{e}^{\mathrm{tr}}\| = 0$ (discussed in Section 2.1), in the time discrete setting, for the case $\|\mathbf{e}^{\mathrm{tr}}\| = \varepsilon_L$, the authors define:

$$F^{TR} = \|\mathbf{X}^{TR}\| - R = \|\hat{\mathbf{s}} + \hat{\gamma}\mathbf{n}^{TR}\| - R \tag{20}$$

 

with

$$\begin{cases} \mathbf{n}^{TR} = \dfrac{\mathbf{e}^{\mathrm{tr},\,TR}}{\|\mathbf{e}^{\mathrm{tr},\,TR}\|} \\ \hat{\mathbf{s}} = \mathbf{s}^{TR} - [\tau_M(T) + h\|\mathbf{e}^{\mathrm{tr},\,TR}\|]\mathbf{n}^{TR} \\ \hat{\gamma} = \langle \hat{\mathbf{s}} \cdot \mathbf{n}^{TR} \rangle \end{cases} \tag{21}$$

They show that if $F^{TR} < 0$, the solution of the set of non-linear equations in the saturated condition (Equation (19)) can be avoided. This approach simplify the calculus, but, at the same time, it makes the limit function $F^{TR}$, and consequently $\mathbf{X}$, not continuous. Indeed, $\|\mathbf{X}\| = R$ during the evolving phase transformation (CASE $PT_1$), while, during the saturated phase case described above, it is $\|\mathbf{X}\| \neq R$: in a monotonic case, for example, it results $\|\mathbf{X}\| = 0$.

- *Non-linear problem solution*: Souza *et al.* suggest to solve Equations (18) and (19) with a Newton-type method, but they do not discuss the starting values for the unknowns during the iterative procedure. In particular, the most obvious choice for $\mathbf{e}^{\mathrm{tr},\,k}$, with the iteration index $k$ equal to 1, would be $\mathbf{e}^{\mathrm{tr},\,1} = \mathbf{e}_n^{\mathrm{tr}}$; however, this choice is not possible since the term $\|\mathbf{e}^{\mathrm{tr},\,1} - \mathbf{e}_n^{\mathrm{tr}}\|$, present in the denominator, would be equal to zero.

## 3. MODIFIED MODEL AND SOLUTION ALGORITHM

Motivated by some of the limits inherent in the model as well as in the proposed time-discrete algorithm, in the present section we suggest some modifications directly on the model, as well as we discuss a robust solution algorithm and the algorithmically consistent tangent.

*Modified model*: The modification, we propose on the model, is relative to the fact that the transformation stress $\mathbf{X}$ and, consequently, $F$ are not defined for the case $\|\mathbf{e}^{\mathrm{tr}}\| = 0$. With respect to this aspect Souza *et al.* investigate the nucleation condition and define $\mathbf{X}$ as

$$\mathbf{X} = R\,\frac{\mathbf{s}}{\|\mathbf{s}\|} \tag{22}$$

just at the onset of the phase transformation. We propose to define $\mathbf{X}$ as

$$\mathbf{X} = \mathbf{s} - (\tau_M + \delta)\frac{\mathbf{s}}{\|\mathbf{s}\|} \tag{23}$$

and to extend this definition over the whole range characterized by $\|\mathbf{e}^{\mathrm{tr}}\| = 0$ and not only to the phase transformation threshold. Assuming to deal with a material characterized by an initial unstressed, unstrained and fully austenitic configuration, we define the scalar internal variable $\delta$ as

$$\delta = \langle \|\mathbf{s}\| - \langle \tau_M - R \rangle^+ \rangle^- \tag{24}$$

 

where $\langle \bullet \rangle^-$ is the function returning the negative part of the argument. Accordingly to Equation (24), for the case $\|\mathbf{e}^{\mathrm{tr}}\| = 0$, it is interesting to observe that:

- If $\tau_M < R$ (i.e. we are in the SME range), $\delta$ is identically zero.
- If $\tau_M > R$ (i.e. we are in the PE range), one of the following situations may occur:

$$
\begin{array}{llll}
\text{if} & \|\mathbf{s}\| = 0 & \text{then } \delta = -(\tau_M - R) & \|\mathbf{X}\| = R \\
\text{if} & 0 < \|\mathbf{s}\| < \tau_M - R & \text{then } \delta = \|\mathbf{s}\| - (\tau_M - R) & \|\mathbf{X}\| = R \\
\text{if} & \tau_M - R < \|\mathbf{s}\| < \tau_M & \text{then } \delta = 0 & \|\mathbf{X}\| = -\|\mathbf{s}\| + \tau_M \\
\text{if} & \tau_M < \|\mathbf{s}\| < \tau_M + R & \text{then } \delta = 0 & \|\mathbf{X}\| = \|\mathbf{s}\| - \tau_M \\
\text{if} & \|\mathbf{s}\| = \tau_M + R & \text{then } \delta = 0 & \|\mathbf{X}\| = R
\end{array}
$$

We observe that, according to the above comments, $\mathbf{X}$ and $F$ (being $F = \|\mathbf{X}\| - R$) are well defined not only at the phase transformation onset, but over the all range with $\|\mathbf{e}^{\mathrm{tr}}\| = 0$.

*Modified algorithm*: Furthermore, as stated at the beginning of the present section, we propose also a solution algorithm modified with respect to the one originally proposed by Souza *et al.* [17]. Still based on an elastic predictor (trial state) inelastic corrector, the modified algorithm distinguish only two cases (Table VI):

- The material is completely in the parent phase ($\|\mathbf{e}_n^{\mathrm{tr}}\| = 0$).
- The material is not completely in the parent phase ($\|\mathbf{e}_n^{\mathrm{tr}}\| > 0$).

In particular, for the case $\|\mathbf{e}_n^{\mathrm{tr}}\| = 0$, we assume that the step is always elastic unless the nucleation condition ($\|\mathbf{s}^{TR}\| \geqslant \tau_M + R$) is satisfied. Accordingly, we may distinguish the following situations:

$$
(1)\ \|\mathbf{s}^{TR}\| \leqslant \tau_M - R \quad \Rightarrow \quad \begin{cases} \delta = \|\mathbf{s}^{TR}\| - \tau_M + R \\ \|\mathbf{X}^{TR}\| = R \\ F^{TR} = 0 \end{cases}
$$

$$
(2)\ \tau_M - R < \|\mathbf{s}^{TR}\| < \tau_M \quad \Rightarrow \quad \begin{cases} \delta = 0 \\ \|\mathbf{X}^{TR}\| = -\|\mathbf{s}\| + \tau_M \\ F^{TR} = -\|\mathbf{s}\| + \tau_M - R < 0 \end{cases}
$$

$$
(3)\ \tau_M < \|\mathbf{s}^{TR}\| < \tau_M + R \quad \Rightarrow \quad \begin{cases} \delta = 0 \\ \|\mathbf{X}^{TR}\| = \|\mathbf{s}\| - \tau_M \\ F^{TR} = \|\mathbf{s}\| - \tau_M - R < 0 \end{cases}
$$

$$
(4)\ \|\mathbf{s}^{TR}\| = \tau_M + R \quad \Rightarrow \quad \begin{cases} \delta = 0 \\ \|\mathbf{X}^{TR}\| = R \\ F^{TR} = 0 \end{cases}
$$

 

Table V. Original time-discrete frame: branch solution and detection of the new state.

Branch Solution and State Update
if (CASE $EL$ – Elastic step) then

$$\begin{cases} \mathbf{e}^{\mathrm{tr}} = \mathbf{e}^{\mathrm{tr},TR} \\ \mathbf{s} = 2G(\mathbf{e} - \mathbf{e}^{\mathrm{tr}}) \\ \text{exit} \end{cases}$$

else if (CASE $PT_1$ – Evolving phase transformation) then

$$\begin{cases} \text{Find } \mathbf{e}^{\mathrm{tr}} \text{ solving: } \mathbf{R}^6(\mathbf{e}^{\mathrm{tr}}) = \mathbf{0} & \text{(See Equation (18))} \\ \text{Check solution: } \begin{cases} \text{if } \|\mathbf{e}^{\mathrm{tr}}\| < \varepsilon_L \text{ then} & \text{exit} \\ \text{else} & \text{CASE } PT_2 \\ \text{end if} \end{cases} \end{cases}$$

else if (CASE $PT_2$ – Saturated phase transformation) then

$$\begin{cases} \text{Find } \mathbf{e}^{\mathrm{tr}}, \gamma \text{ solving: } \mathbf{R}^7(\mathbf{e}^{\mathrm{tr}}, \gamma) = \mathbf{0} & \text{(See Equation (19))} \\ \text{exit} \end{cases}$$

end if

We note that:

- Case 1 represents an elastic step, in the sense that no phase transformation is active since $F^{TR} = 0$ but the nucleation condition cannot be satisfied.
- Cases 2 and 3 still represents an elastic step since $F^{TR} < 0$.
- Case 4 represents the onset of the phase transformation, since $F^{TR} = 0$ and, at the same time, the phase transformation nucleation condition is satisfied.

Besides the different expression for $\mathbf{X}$ introduced to obtain an extended range of definition for such a variable, more significative differences between the proposed modified algorithm with respect to the original algorithm are in the solution of the non-linear evolutionary problem. In particular, for the case $\|\mathbf{e}_n^{\mathrm{tr}}\| = 0$ when the nucleation condition is satisfied or for the case $\|\mathbf{e}_n^{\mathrm{tr}}\| > 0$ when $F^{TR} > 0$, we suggest the following procedure (Table VI):

- Assume $\gamma = 0$, and rewrite Equation (17) in the residual form as follows:

$$\tilde{\mathbf{R}}^7(\mathbf{X}, \Delta\zeta) = \begin{cases} \mathbf{X} - \mathbf{s}^{TR} + 2G\Delta\zeta \dfrac{\mathbf{X}}{\|\mathbf{X}\|} + [\tau_M(T) + h\|\mathbf{e}^{\mathrm{tr}}\|] \dfrac{\mathbf{e}^{\mathrm{tr}}}{\|\mathbf{e}^{\mathrm{tr}}\|} = \mathbf{0} \\ \|\mathbf{X}\| - R = 0 \end{cases} \tag{25}$$

where $\mathbf{e}^{\mathrm{tr}} = \mathbf{e}_n^{\mathrm{tr}} + \Delta\zeta/(\mathbf{X}/\|\mathbf{X}\|)$ (Equation (17d)).

Then, these seven non-linear scalar equations are solved with a Newton–Raphson method.

 

Table VI. Modified time-discrete frame: detection of the material state and of the evolution branch.

State and Branch Detection

if $(\|\mathbf{e}_n^{\mathrm{tr}}\| = 0)$ then

$$\begin{cases} \text{compute:} & \begin{cases} \boldsymbol{\alpha}^{TR} = (\tau_M(T) + \delta)\dfrac{\mathbf{s}^{TR}}{\|\mathbf{s}^{TR}\|} \\ \mathbf{X}^{TR} = \mathbf{s}^{TR} - \boldsymbol{\alpha}^{TR} \\ F^{TR} = \|\mathbf{X}^{TR}\| - R \end{cases} \\ \text{check } F^{TR}\text{:} & \begin{cases} \text{if } (F^{TR} < 0) \text{ or } (F^{TR} = 0 \\ \quad \text{and } \|\mathbf{s}\| < \tau_M + R) \text{ then} & \textbf{elastic step } (EL) \\ \text{else} & \textbf{active p.t. } (PT_1) \\ \text{end if} \end{cases} \end{cases} \tag{48}$$

else

$$\begin{cases} \text{compute:} & \begin{cases} \boldsymbol{\alpha}^{TR} = [\tau_M(T) + h\|\mathbf{e}^{\mathrm{tr},\,TR}\|]\mathbf{n}^{TR} \\ \mathbf{X}^{TR} = \mathbf{s}^{TR} - \boldsymbol{\alpha} TR \\ F^{TR} = \|\mathbf{X}^{TR}\| - R \end{cases} \\ \text{check } F^{TR}\text{:} & \begin{cases} \text{if } (F^{TR} < 0) \text{ then} & \textbf{elastic step } (EL) \\ \text{else} & \textbf{active p.t. } (PT_1) \\ \text{endif} \end{cases} \end{cases} \tag{49}$$

end if

- If the above solution is non-admissible $(\|\mathbf{e}^{\mathrm{tr}}\| > \varepsilon_L)$, assume $\gamma > 0$ and rewrite Equation (17) in the residual form as follows:

$$\tilde{\mathbf{R}}^8(\mathbf{X}, \Delta\zeta, \gamma) = \begin{cases} \mathbf{X} - \mathbf{s}^{TR} + 2G\Delta\zeta\,\dfrac{\mathbf{X}}{\|\mathbf{X}\|} + [\tau_M(T) + h\|\mathbf{e}^{\mathrm{tr}}\| + \gamma]\dfrac{\mathbf{e}^{\mathrm{tr}}}{\|\mathbf{e}^{\mathrm{tr}}\|} = \mathbf{0} \\ \|\mathbf{X}\| - R = 0 \\ \|\mathbf{e}^{\mathrm{tr}}\| - \varepsilon_L = 0 \end{cases} \tag{26}$$

  Then, these eight non-linear scalar equations can be solved with a Newton–Raphson method.

*Comments on features of the modified algorithm*: To overcome the original model limits underlined in Section 2.2, we proposed a new definition of the transformation stress and an efficient method for the non-linear problem solution. In the following the two modifications, presented in the previous section, will be discussed.

- The nucleation condition proposed in the modified algorithm can be derived considering the case of active phase transformation and $\|\mathbf{e}^{\mathrm{tr}}\| \to 0$. In fact, in a time-continuous frame,

 

during phase transformation, from Equations (7), (8) and (12) we have:

$$\begin{cases} \dot{\mathbf{e}}^{\mathrm{tr}} \neq 0 \\ \|\mathbf{X}\| = R \\ \dfrac{\dot{\mathbf{e}}^{\mathrm{tr}}}{\|\dot{\mathbf{e}}^{\mathrm{tr}}\|} = \dfrac{\mathbf{X}}{\|\mathbf{X}\|} \\ \dfrac{\mathbf{e}^{\mathrm{tr}}}{\|\mathbf{e}^{\mathrm{tr}}\|} = \dfrac{\mathbf{s}-\mathbf{X}}{\|\mathbf{s}-\mathbf{X}\|} \end{cases} \tag{27}$$

Indicating with 0 the time corresponding to the phase transformation onset and considering an instant of time $T>0$, we have:

$$\frac{\mathbf{e}^{\mathrm{tr}}}{\|\mathbf{e}^{\mathrm{tr}}\|} \approx \frac{\dot{\mathbf{e}}^{\mathrm{tr}}}{\|\dot{\mathbf{e}}^{\mathrm{tr}}\|} \approx \frac{\mathbf{X}}{\|\mathbf{X}\|} \approx \frac{\mathbf{s}}{\|\mathbf{s}\|} \tag{28}$$

where the approximation errors go to zero when $T \to 0$. Considering the limit of relation 28, at the nucleation condition, ($\|\mathbf{e}^{\mathrm{tr}}\| = 0$) we may set:

$$\begin{cases} \mathbf{X} = \mathbf{s} - \left[\tau_M(T)\dfrac{\mathbf{s}}{\|\mathbf{s}\|}\right] \\ F = \|\mathbf{s}\| - [\tau_M(T) + R] = 0 \end{cases} \tag{29}$$

which represents the nucleation condition.

- Using Equation (24) for the case $\|\mathbf{e}^{\mathrm{tr}}\| = 0$, the variable $\mathbf{X}$ is now always defined (except in the point $\|\mathbf{s}\| = 0$), rendering the overall numerical solution more consistent and stable.
- The non-linear Equations (25) and (26) are in general solved through a Newton–Raphson iteration method. It is interesting to observe that we eliminated the problems present in the original algorithm relative to the starting values for the iterations. As an example, for Equation (26), it is possible to start from the most obvious choice for $\mathbf{e}^{\mathrm{tr},k}$, $\Delta\zeta^k$, $\gamma^k$, with the iteration index $k$ equal to 1, that is $\mathbf{e}^{\mathrm{tr},1} = \mathbf{e}_n^{\mathrm{tr}}$, $\Delta\zeta^1 = 0$, $\gamma^1 = \gamma_n$. Similar conditions are valid for the solution of Equation (25).

As final remark we note that the suggested procedure falls only in the case of $\mathbf{e}_n^{\mathrm{tr}} = 0$. However, for such a case we introduce a tentative value of $\mathbf{e}^{\mathrm{tr}}$; in fact, since:

$$\mathbf{s}^{TR} = 2G(\mathbf{e} - \mathbf{e}^{\mathrm{tr},TR}) \tag{30}$$

defined $\tilde{\mathbf{n}} = \mathbf{s}^{TR}/\|\mathbf{s}^{TR}\|$, Equation (28) implies:

$$(\|\mathbf{s}^{TR}\| + 2G\|\mathbf{e}^{\mathrm{tr},TR}\|)\tilde{\mathbf{n}} = 2G\mathbf{e} \tag{31}$$

Hence, $\mathbf{e}$ and $\mathbf{s}^{TR}$ are parallel in the nucleation phase, and we can define:

$$\|\mathbf{e}^{\mathrm{tr},TR}\| = \|\mathbf{e}\| - \frac{\|\mathbf{s}^{TR}\|}{2G} = \|\mathbf{e}\| - \frac{\tau_M(T) + R}{2G} \tag{32}$$

Finally, we can set $\mathbf{e}^{\mathrm{tr},1} = \mathbf{e}^{\mathrm{tr},TR}$ when $\mathbf{e}_n^{\mathrm{tr}} = 0$.

 

### 3.1. Newton–Raphson method

As stated, we solve the non-linear Equations (25) and (26) with a Newton–Raphson method. Accordingly, we need to detail the form of the corresponding tangent matrix. For brevity, we report the construction of the tangent only for the case of the saturated phase transformation (corresponding to Equation (26)), since the case of the non-saturated phase transformation can be obtained simply eliminating the last row. Linearizing Equation (26), we find:

$$\begin{cases} d(\mathbf{R}^X) = \mathbf{R}^X_{,X} : \mathrm{d}\mathbf{X} + \mathbf{R}^X_{,\Delta\zeta}\, \mathrm{d}\Delta\zeta + \mathbf{R}^X_{,\gamma}\, \mathrm{d}\gamma \\ d(R^{\Delta\zeta}) = \mathbf{R}^{\Delta\zeta}_{,X} : \mathrm{d}\mathbf{X} + R^{\Delta\zeta}_{,\Delta\zeta}\, \mathrm{d}\Delta\zeta + R^{\Delta\zeta}_{,\gamma}\, \mathrm{d}\gamma \\ d(R^{\gamma}) = \mathbf{R}^{\gamma}_{,X} : \mathrm{d}\mathbf{X} + R^{\gamma}_{,\Delta\zeta}\, \mathrm{d}\Delta\zeta + R^{\gamma}_{,\gamma}\, \mathrm{d}\gamma \end{cases} \tag{33}$$

where

$$\begin{aligned} \mathbf{R}^X_{,X} &= \mathbb{I} + (2G + h)\Delta\zeta\mathbb{B}^X + (\tau_M + \gamma)\Delta\zeta\mathbb{B}^e\,\mathbb{B}^X \\ \mathbf{R}^X_{,\Delta\zeta} &= (2G + h)\mathbf{N}^X + (\tau_M + \gamma)\mathbb{B}^e : \mathbf{N}^X \\ \mathbf{R}^X_{,\gamma} &= \mathbf{N}^e \\ \mathbf{R}^{\Delta\zeta}_{,X} &= \mathbf{N}^X \\ R^{\Delta\zeta}_{,\Delta\zeta} &= 0 \\ R^{\Delta\zeta}_{,\gamma} &= 0 \\ \mathbf{R}^{\gamma}_{,X} &= \Delta\zeta\mathbb{B}^X : \mathbf{N}^e \\ R^{\gamma}_{,\Delta\zeta} &= \mathbf{N}^e : \mathbf{N}^X \\ R^{\gamma}_{,\gamma} &= 0 \end{aligned}$$

with

$$\begin{aligned} \mathbf{N}^X &= \frac{\mathbf{X}}{\|\mathbf{X}\|} \\ \mathbf{N}^e &= \frac{\mathbf{e}^{\mathrm{tr}}}{\|\mathbf{e}^{\mathrm{tr}}\|} \\ \mathbb{B}^X &= \frac{1}{\|\mathbf{X}\|}[\mathbb{I} - \mathbf{N}^X \otimes \mathbf{N}^X] \\ \mathbb{B}^e &= \frac{1}{\|\mathbf{e}^{\mathrm{tr}}\|}[\mathbb{I} - \mathbf{N}^e \otimes \mathbf{N}^e] \end{aligned}$$

and $\mathbb{I}$ indicates the fourth-order identity tensor.[†]

[†]The notation $\mathbb{A}$ is used for a general fourth-order tensor, while $\mathbf{A}$ indicates a second-order tensor. The notation $X_{,Y}$ means $\partial X/\partial Y$.

 

### 3.2. Consistent tangent matrix

We now address the construction of the tangent tensor consistent with the modified discrete model. The use of a consistent tangent tensor preserves the quadratic convergence of the Newton–Raphson method, for the incremental solution of the global time-discrete problem, as it is common done in the framework of a finite element scheme.

The consistent tangent can be computed as a linearization of the stress $\boldsymbol{\sigma}$:

$$\mathbb{D} = \frac{\mathrm{d}\boldsymbol{\sigma}}{\mathrm{d}\boldsymbol{\varepsilon}} \tag{34}$$

Recalling Equations (5) and (6), the linearization of the elastic constitutive relation, in its volumetric and deviatoric component, gives:

$$\begin{aligned} \mathrm{d}p\,\mathbf{1} &= K(\mathbf{1}\otimes\mathbf{1}) : \mathrm{d}\boldsymbol{\varepsilon} \\ \mathrm{d}\mathbf{s} &= 2G\left(\mathbb{I} - \frac{\mathrm{d}\mathbf{e}^{\mathrm{tr}}}{\mathrm{d}\mathbf{e}}\right)\mathbb{I}_{\mathrm{dev}} : \mathrm{d}\boldsymbol{\varepsilon} \end{aligned} \tag{35}$$

where

$$\begin{aligned} \mathbb{I}_{\mathrm{dev}} &= \mathbb{I} - \tfrac{1}{3}(\mathbf{1}\otimes\mathbf{1}) \\ \mathrm{d}\mathbf{e} &= \mathbb{I}_{\mathrm{dev}} : \mathrm{d}\boldsymbol{\varepsilon} \end{aligned}$$

with $\mathbf{1}$ the second-order identity tensor. If we now consider Equation (26) as function of $\mathbf{X}$, $\Delta\zeta$, $\gamma$ and $\mathbf{e}$, the corresponding linearization gives:

$$\begin{aligned} d(\mathbf{R}^X) &= \mathbf{R}^X_{,X} : \mathrm{d}\mathbf{X} + \mathbf{R}^X_{,\Delta\zeta}\,\mathrm{d}\Delta\zeta + \mathbf{R}^X_{,\gamma}\,\mathrm{d}\gamma + \mathbf{R}^X_{,\mathbf{e}} : \mathrm{d}\mathbf{e} = \mathbf{0} \\ d(R^{\Delta\zeta}) &= \mathbf{R}^{\Delta\zeta}_{,X} : \mathrm{d}\mathbf{X} + R^{\Delta\zeta}_{,\Delta\zeta}\,\mathrm{d}\Delta\zeta + R^{\Delta\zeta}_{,\gamma}\,\mathrm{d}\gamma + \mathbf{R}^{\Delta\zeta}_{,\mathbf{e}} : \mathrm{d}\mathbf{e} = 0 \\ d(R^{\gamma}) &= \mathbf{R}^{\gamma}_{,X} : \mathrm{d}\mathbf{X} + R^{\gamma}_{,\Delta\zeta}\,\mathrm{d}\Delta\zeta + R^{\gamma}_{,\gamma}\,\mathrm{d}\gamma + \mathbf{R}^{\gamma}_{,\mathbf{e}} : \mathrm{d}\mathbf{e} = 0 \end{aligned} \tag{36}$$

where

$$\begin{aligned} \mathbf{R}^X_{,\mathbf{e}} &= -2G\mathbb{I} \\ \mathbf{R}^{\Delta\zeta}_{,\mathbf{e}} &= \mathbf{0} \\ \mathbf{R}^{\gamma}_{,\mathbf{e}} &= \mathbf{0} \end{aligned}$$

Accordingly, we can write:

$$\begin{bmatrix} \mathrm{d}\mathbf{X} \\ \mathrm{d}\Delta\zeta \\ \mathrm{d}\gamma \end{bmatrix} = \begin{bmatrix} \mathbf{R}^X_{,X} & \mathbf{R}^X_{,\Delta\zeta} & \mathbf{R}^X_{,\gamma} \\ \mathbf{R}^{\Delta\zeta}_{,X} & R^{\Delta\zeta}_{,\Delta\zeta} & R^{\Delta\zeta}_{,\gamma} \\ \mathbf{R}^{\gamma}_{,X} & R^{\gamma}_{,\Delta\zeta} & R^{\gamma}_{,\gamma} \end{bmatrix}^{-1} \begin{bmatrix} -2G\mathbb{I} \\ \mathbf{0} \\ \mathbf{0} \end{bmatrix} : \mathrm{d}\mathbf{e} \tag{37}$$

 

The linearization of Equation (17d) gives:

$$d(\mathbf{e}^{\mathrm{tr}}) = \mathbf{e}^{\mathrm{tr}}_{,X} : \mathrm{d}\mathbf{X} + \mathbf{e}^{\mathrm{tr}}_{,\Delta\zeta}\, \mathrm{d}\Delta\zeta + \mathbf{e}^{\mathrm{tr}}_{,\gamma}\, \mathrm{d}\gamma \tag{38}$$

Since

$$\begin{aligned} \mathbf{e}^{\mathrm{tr}}_{,X} &= \Delta\zeta \mathbb{B}^{X} \\ \mathbf{e}^{\mathrm{tr}}_{,\Delta\zeta} &= \frac{\mathbf{X}}{\|\mathbf{X}\|} \\ \mathbf{e}^{\mathrm{tr}}_{,\gamma} &= \mathbf{0} \end{aligned} \tag{39}$$

we have

$$d(\mathbf{e}^{\mathrm{tr}}) = \mathbb{E} : \mathrm{d}\mathbf{e} \tag{40}$$

with

$$\mathbb{E} = \begin{bmatrix} \Delta\zeta \mathbb{B}^{X} & \dfrac{\mathbf{X}}{\|\mathbf{X}\|} & \mathbf{0} \end{bmatrix}^{\mathrm{T}} \begin{bmatrix} \mathbf{R}^{X}_{,X} & \mathbf{R}^{X}_{,\Delta\zeta} & \mathbf{R}^{X}_{,\gamma} \\ \mathbf{R}^{\Delta\zeta}_{,X} & R^{\Delta\zeta}_{,\Delta\zeta} & R^{\Delta\zeta}_{,\gamma} \\ \mathbf{R}^{\gamma}_{,X} & R^{\gamma}_{,\Delta\zeta} & R^{\gamma}_{,\gamma} \end{bmatrix}^{-1} \begin{bmatrix} -2G\mathbb{I} \\ \mathbf{0} \\ \mathbf{0} \end{bmatrix}$$

In conclusion, the consistent tangent tensor assumes the form:

$$\mathbb{D} = K(\mathbf{1} \otimes \mathbf{1}) + 2G(\mathbb{I} - \mathbb{E})\mathbb{I}_{\mathrm{dev}} \tag{41}$$

## 4. NUMERICAL EXAMPLES

The model ability to reproduce the basic SMA features was already proved by Souza *et al.* through several numerical tests. In particular, they consider a material with properties:

$$E = 70\,000 \text{ MPa}, \quad R = 45 \text{ MPa}, \quad h = 500 \text{ MPa}, \quad v = 0.33$$
$$\beta = 7.5 \text{ MPa K}^{-1}, \quad T_0 = 253.15 \text{ K}, \quad \varepsilon_L = 0.03$$

and performed the following tests:

TEST A isothermal strain-driven uni-axial (tension-compression) test.
TEST B isothermal uni-axial tensile test (loading-unloading), followed by a stress-free thermal cycle.
TEST C temperature-driven uni-axial test under prescribed stress level.

Moreover, they compared the model response with the non-proportional experimental tests described in Reference [28], showing the good performance of the model.

To prove the robustness and effectiveness of our modified algorithm, we repeat this first set of analyses (also with large time integration step), obtaining the same $\boldsymbol{\sigma} - \boldsymbol{\varepsilon} - T$ curves reported by Souza *et al.* [17].

 

Table VII. Modified time-discrete frame: branch solution and detection of the new state.

Branch Solution and State Update

if (CASE $EL$ – Elastic step) then

$$\begin{cases} \mathbf{e}^{\mathrm{tr}} = \mathbf{e}^{\mathrm{tr},\,TR} \\ \mathbf{s} \;\; = 2G(\mathbf{e} - \mathbf{e}^{\mathrm{tr}}) \\ \text{exit} \end{cases}$$

else if (CASE $PT_1$ – Evolving phase transformation) then

$$\begin{cases} \text{Find } \mathbf{e}^{\mathrm{tr}} \text{ solving: } \tilde{\mathbf{R}}^{7}(\mathbf{X}, \Delta\zeta) = \mathbf{0} & \text{(See Equation (25))} \\ \text{Check solution: } \begin{cases} \text{if } \|\mathbf{e}^{\mathrm{tr}}\| < \varepsilon_L \text{ then} & \text{exit} \\ \text{else} & \text{CASE } PT_2 \\ \text{end if} \end{cases} \end{cases}$$

else if (CASE $PT_2$ – Saturated phase transformation) then

$$\begin{cases} \text{Find } \mathbf{e}^{\mathrm{tr}},\ \gamma \text{ solving: } \quad \tilde{\mathbf{R}}^{8}(\mathbf{X}, \Delta\zeta, \gamma) = \mathbf{0} & \text{(See Equation (26))} \\ \text{exit} \end{cases}$$

end if

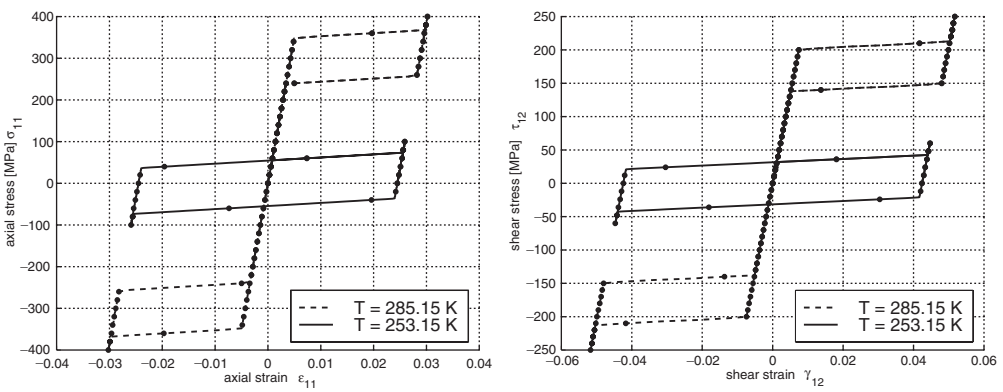


Figure 1. Modified solution algorithm. Tension–compression tests (left part): $T = 285.15$ K—integration time step 0.01 s (line) and 0.05 s (dot); $T = 253.15$ K—integration time step 0.01 s (line) and 0.2 s (dot). Torsion tests (right part): $T = 285.15$ K—integration time step 0.01 s (line) and 0.04 s (dot); $T = 253.15$ K—integration time step 0.01 s (line) and 0.2 s (dot).

Then, we consider a second set of numerical tests to verify even in more detail the efficiency of the modified algorithm. Using again the material parameters suggested by Souza, we investigate both uni-axial and multi-axial (non-proportional) tests.

 

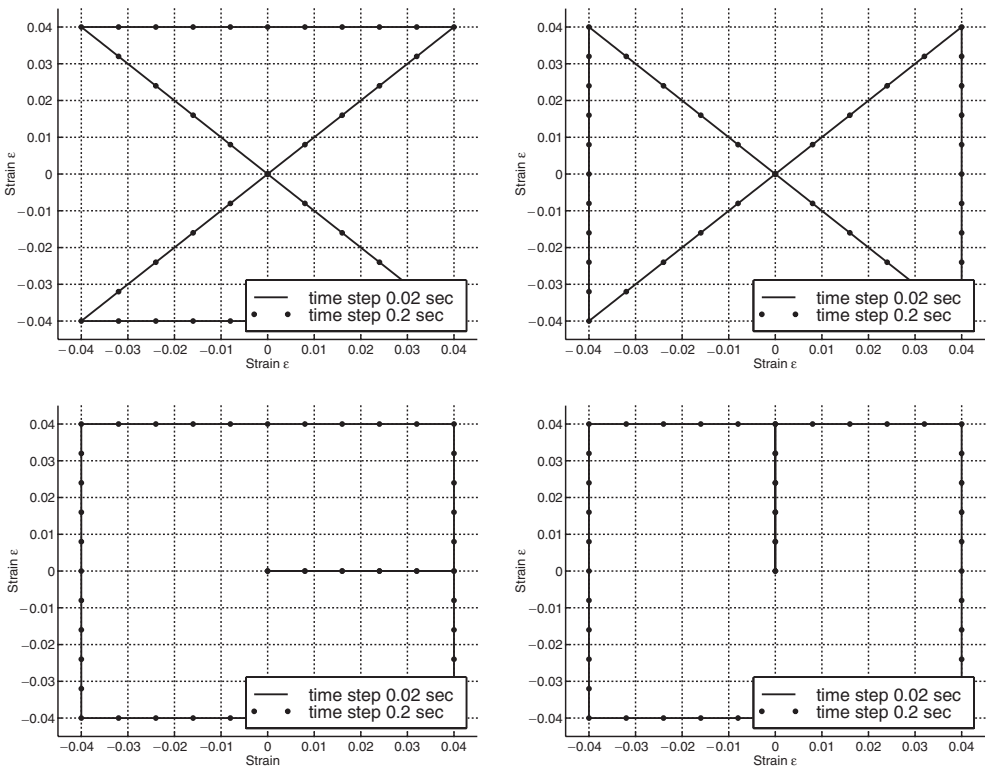


Figure 2. Bi-axial test. *Hourglass* test strain histories: type $A_h$ (upper left), type $B_h$ (upper right); *Square* test strain histories: type $A_s$ (lower left), type $B_s$ (lower right).

Different time steps sizes are adopted to check the algorithm implementation. The non-linear problem solution is characterized by two different iteration processes: one assures the reaching of the global equilibrium (*global solution process*); the other assures the satisfaction of the model for each tentative strain (*local solution process*). Moreover, recalling the proposed algorithm (Table VII), we distinguish between two local solution processes: they search a solution that satisfies the CASE $PT_1$ condition ($PT_1$ *local solution process*) and the CASE $PT_2$ condition ($PT_2$ *local solution process*), respectively.

The following quantities are calculated to define the global and local convergence performance:

- Number of steps adopted to describe the loading history ($S$).
- Total number of iterations during the global solution process ($I$).
- Number of iterations during $PT_1$ local solution process ($I_1$).
- Number of iterations during $PT_2$ local solution process ($I_2$).
- Average number of iterations during the global solution process ($I/S$).
- Average number of iterations during $PT_1$ local solution process ($I_1/S$).
- Average number of iterations during $PT_2$ local solution process ($I_2/S$).

 

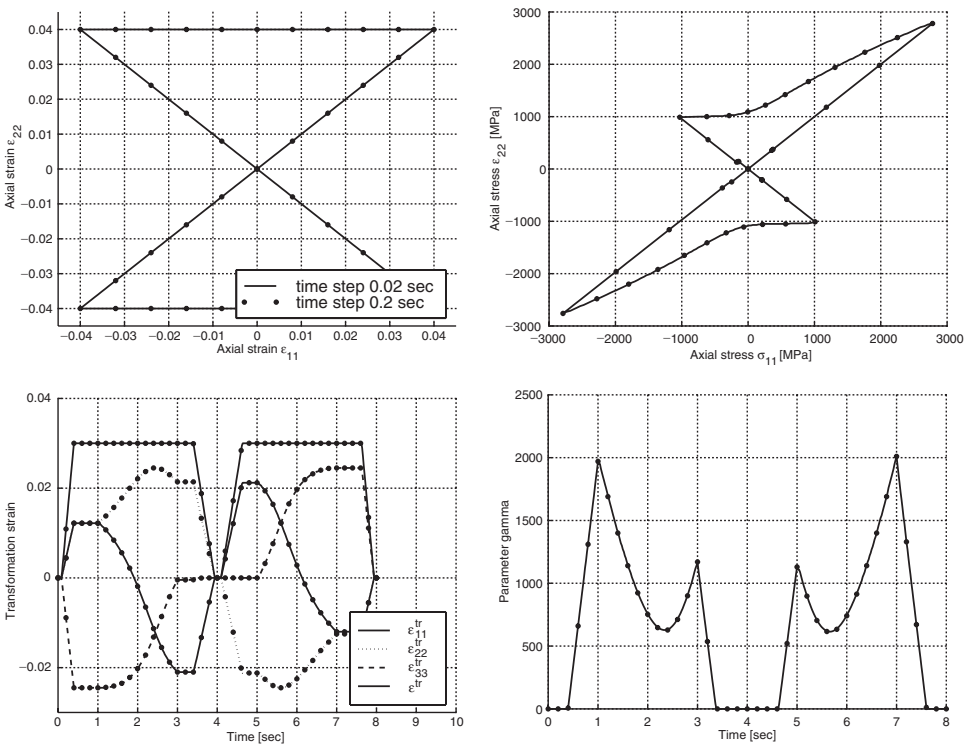


Figure 3. $\varepsilon_{11} - \varepsilon_{22}$ $A_h$ test. Strain history input (upper left); stress history output (upper right); transformation strain history (lower left); $\gamma$ parameter history (lower right).

### *4.1. Uni-axial tests*

Cyclic tension and torsion tests under stress control ($\sigma_{11}$ and $\tau_{12}$, respectively, are varied, while the non-controlled stress components are constrained to be zero) are simulated at the following temperatures:

- $T = 253.15$ K: the material is stable in martensitic phase and the shape memory effect takes place.
- $T = 285.15$ K: the material is stable in austenitic phase and the pseudoelasticity takes place.

Figure 1 compares the results for different time integration step size showing the model capability to reproduce the pseudoelasticity and the shape memory effect, as well as its limit to describe a symmetric tension–compression response. To overcome this shortcoming, we are developing an extension of the modified algorithm, as it is summarized in Appendix A.1.

We notice that a 4% deformation induces saturated phase transformation in case of axial stress, but not in case of shear stress: this observation will be useful to explain some results in the multi-axial tests. For each uni-axial test the average number of iterations in the global

 

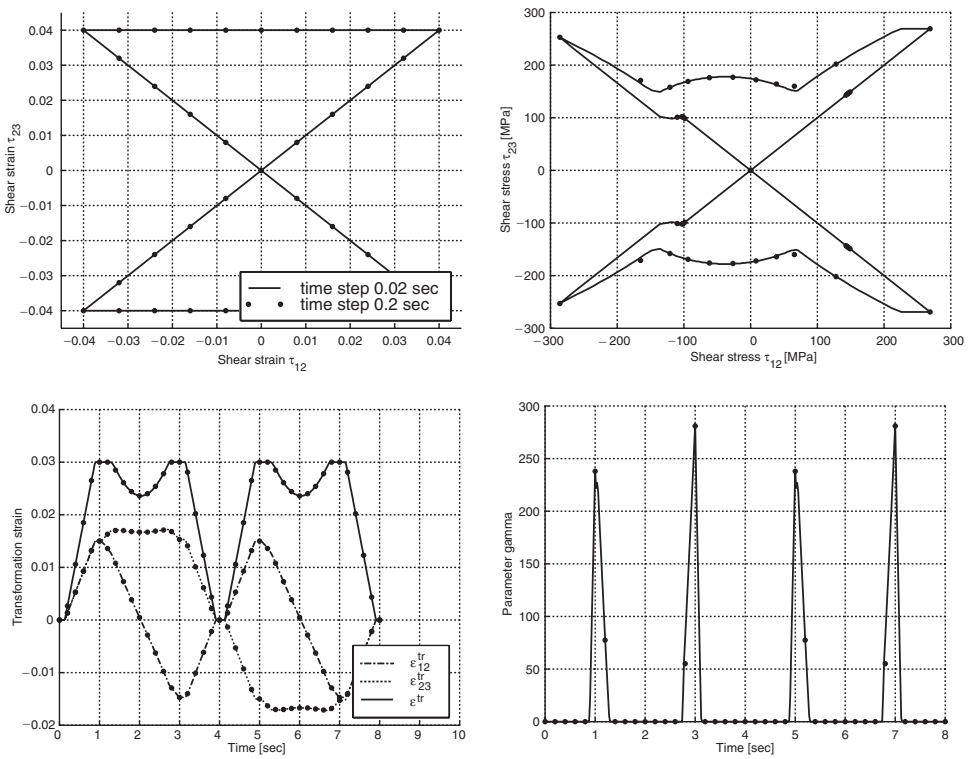


Figure 4. $\varepsilon_{12} - \varepsilon_{23}$ $A_h$ test. Strain history input (upper left); stress history output (upper right); transformation strain history (lower left); $\gamma$ parameter history (lower right).

convergence process is always equal to 2: it points out the model capability to have a very fast convergence (in particular, super-quadratic), even for large time steps.

### 4.2. *Multi-axial tests*

Motivated by the interest to investigate the numerical algorithm performance, as well as the model behaviour in terms of stress-induced mono-variant martensite reorientation under different loading conditions, we perform several strain-driven bi-axial tests.

In particular, four series of isothermal tests are performed varying the time step (0.02 and 0.2 s), the test temperature ($T = 253.15$ and $= 285.15$ K) and the strain components involved. The first two series are characterized by the bi-axial strain histories plotted in the upper part of Figure 2 and in the following indicated as *hourglass* tests, type $A_h$ and $B_h$; the other two series are characterized by the bi-axial strain histories plotted in the lower part of Figure 2 and in the following indicated as the *square* tests, type $A_s$ and $B_s$. For each series the following couples of deformation components are considered: $\varepsilon_{11} - \varepsilon_{22}$; $\varepsilon_{11} - \varepsilon_{12}$; $\varepsilon_{12} - \varepsilon_{23}$. The tests are performed varying the chosen strain components between the range $\pm 4\%$ and keeping equal to zero the stress components corresponding to the non-controlled strains.

In all the cases the modified algorithm has a good performance, as it is shown by the results plotted in the following, relative to the *hourglass* tests at $T = 285.15$ K. In particular,

 

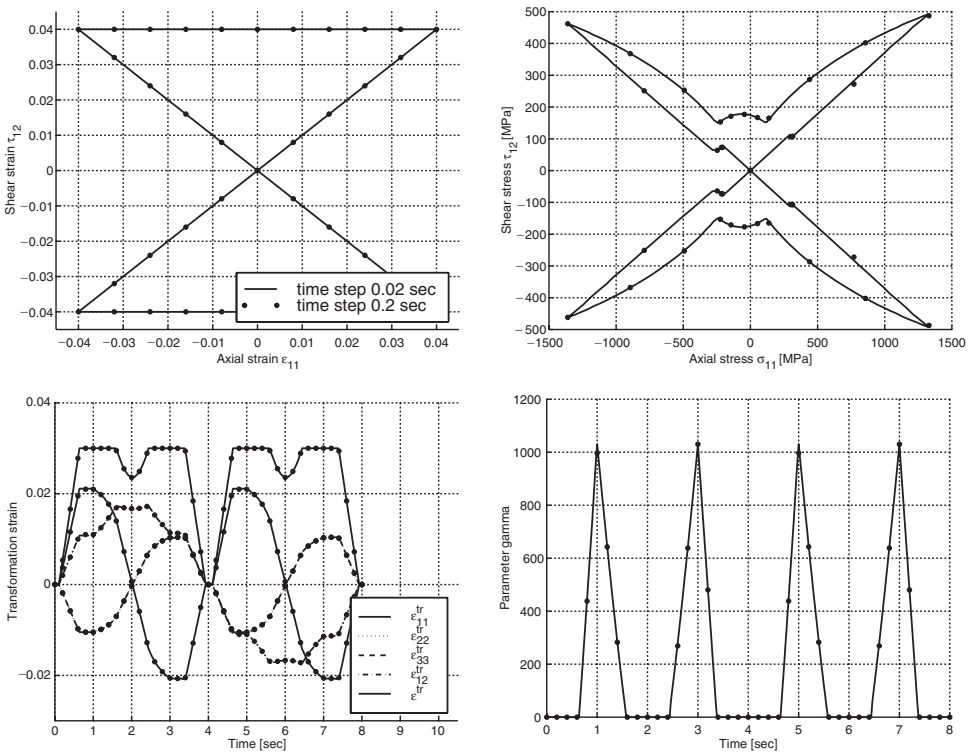


Figure 5. $\varepsilon_{11} - \varepsilon_{12}$ $A_h$ test. Strain history input (upper left); stress history output (upper right); transformation strain history (lower left); $\gamma$ parameter history (lower right).

the strain history, the stress response, the transformation strain and the $\gamma$ parameter history are reported for each test. The expected symmetry between the $A_h$ and $B_h$ test curves for the couple $\varepsilon_{11} - \varepsilon_{22}$ confirms the correct implementation of the algorithm. The same symmetry could be found comparing the $A_h$ and $B_h$ test results for the couple $\varepsilon_{12} - \varepsilon_{23}$: in Figures 3 and 4 the $\varepsilon_{11} - \varepsilon_{22}$ and $\varepsilon_{12} - \varepsilon_{23}$ $A_h$ test responses are shown, respectively. On the other hand, the results of the tests $A_h$ and $B_h$ for the $\varepsilon_{11} - \varepsilon_{12}$ couple, plotted in Figure 5 and 6, respectively, show a strong difference. This behaviour is explained by the coupling among tension and torsion under multi-axial loading: the complete transformation induced in $\varepsilon_{11}$ component and the only partial transformation induced in $\varepsilon_{12}$ component at 4% of deformation return different stress paths for the two strain histories. It is more evident if one considers the $\gamma$ parameter history: (1) case $\varepsilon_{11} - \varepsilon_{12}$ (Figure 5 lower right): during $\varepsilon_{11}$ variation at constant $\varepsilon_{12}$ (time: 1–2, 2–3, 5–6 and 6–7 s), the material undergoes martensite reorientation of the saturated phase and reverse transformation. (2) case $\varepsilon_{12} - \varepsilon_{11}$ (Figure 6 lower right): during $\varepsilon_{12}$ variation at constant $\varepsilon_{11}$ (time: 1–2, 2–3, 5–6 and 6–7 s), only product phase reorientation takes place and the material remains in saturated phase. Moreover, in both the case during proportional increasing–decreasing of axial and shear strain (time: 0–1, 3–5 and 7–8 s) the saturated phase is reached at the same stress value and the product phase undergoes elastic deformation without reorientation ($\gamma$ vary linearly).

 

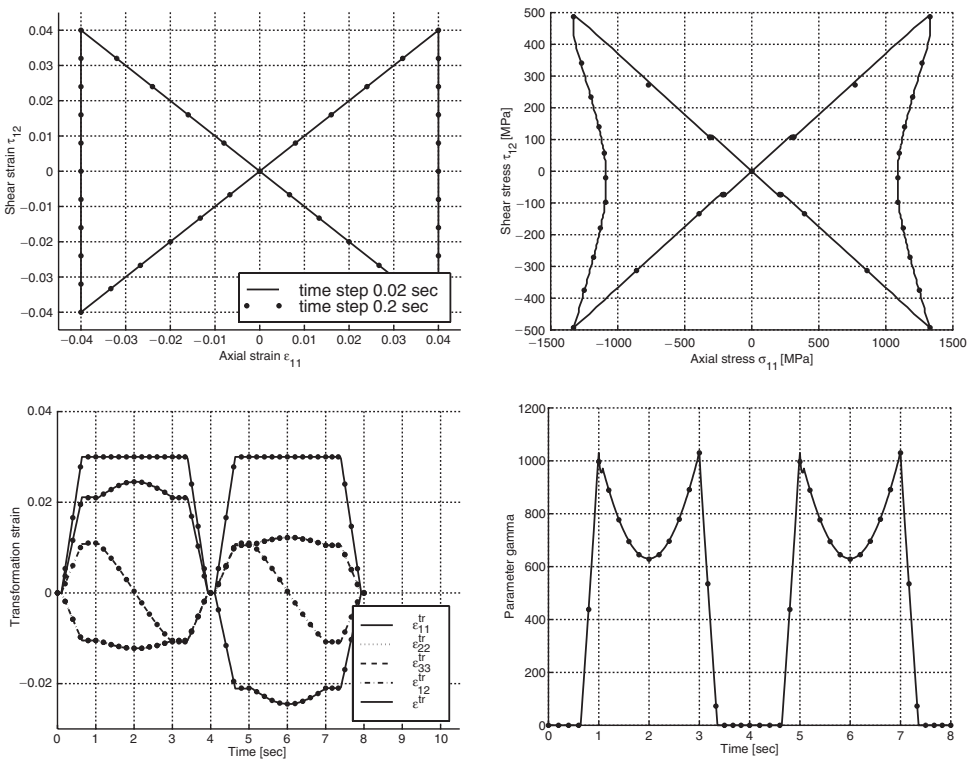


Figure 6. $\varepsilon_{12} - \varepsilon_{11}$ $B_h$ test. Strain history input (upper left); stress history output (upper right); transformation strain history (lower left); $\gamma$ parameter history (lower right).

The performance of the implemented algorithm is checked comparing simulations with 0.02 s (continuous line in the figures) and 0.2 s (dots in the figures) integration time step. The results of the convergence analysis are summarized in Table VIII and Table IX, for all the performed hourglass and square tests, respectively. The average number of iterations per step in the global process is no more than 4, confirming the fast convergence of the model and the efficiency of the algorithm. The performance is worst in the local convergence processes: the average number of iterations goes from 2 to 6 in CASE $PT_1$ and from 5 to 14 in CASE $PT_2$. Actually, the analysis of the residual values shows that, during the evolving and saturated phase transformation, the Newton–Raphson method starts from a point far from the solution: we are studying the possibility to define better initial conditions, to improve the convergence also in the local processes.

## 5. CLOSURE AND FUTURE RESEARCH DIRECTIONS

Motivated by the theoretical potency and, at the same time, simplicity of the 3D model for stress-induced transformations proposed by Souza *et al.* we deeply investigate it. The results

 

Table VIII. Hourglass test convergence.

| Test | Temp. (K) | $S$ | $I$ | $I/S$ | $I_1/S$ | $I_2/S$ |
|---|---|---|---|---|---|---|
| Type $A_h$ | 253.15 | 400 | 1107 | 2 | 2 | 12 |
| $\varepsilon_{11} - \varepsilon_{22}$ | | 40 | 124 | 3 | 2 | 7 |
| | 285.15 | 400 | 1090 | 2 | 5 | 12 |
| | | 40 | 123 | 3 | 5 | 7 |
| Type $B_h$ | 253.15 | 400 | 1107 | 2 | 2 | 12 |
| $\varepsilon_{11} - \varepsilon_{22}$ | | 40 | 124 | 3 | 2 | 7 |
| | 285.15 | 400 | 1090 | 2 | 5 | 12 |
| | | 40 | 123 | 3 | 5 | 7 |
| Type $A_h$ | 253.15 | 400 | 1448 | 3 | 2 | 11 |
| $\varepsilon_{11} - \varepsilon_{12}$ | | 40 | 156 | 3 | 2 | 8 |
| | 285.15 | 400 | 1394 | 3 | 5 | 11 |
| | | 40 | 156 | 3 | 5 | 7 |
| Type $B_h$ | 253.15 | 400 | 1226 | 3 | 2 | 14 |
| $\varepsilon_{11} - \varepsilon_{12}$ | | 40 | 134 | 3 | 2 | 8 |
| | 285.15 | 400 | 1208 | 3 | 5 | 13 |
| | | 40 | 130 | 3 | 5 | 8 |
| Type $A_h$ | 253.15 | 400 | 400 | 1 | 2 | 8 |
| $\varepsilon_{12} - \varepsilon_{23}$ | | 40 | 40 | 1 | 2 | 5 |
| | 285.15 | 400 | 400 | 1 | 4 | 7 |
| | | 40 | 40 | 1 | 4 | 5 |

Table IX. Square test convergence.

| Test | Temp. (K) | $S$ | $I$ | $I/S$ | $I_1/S$ | $I_2/S$ |
|---|---|---|---|---|---|---|
| Type $A_s$ | 253.15 | 500 | 1914 | 3 | 2 | 14 |
| $\varepsilon_{11} - \varepsilon_{22}$ | | 50 | 205 | 4 | 2 | 8 |
| | 285.15 | 500 | 1883 | 3 | 5 | 13 |
| | | 50 | 204 | 4 | 6 | 8 |
| Type $B_s$ | 253.15 | 500 | 1914 | 3 | 2 | 14 |
| $\varepsilon_{11} - \varepsilon_{22}$ | | 50 | 205 | 4 | 2 | 8 |
| | 285.15 | 500 | 1883 | 3 | 5 | 13 |
| | | 50 | 204 | 4 | 6 | 8 |
| Type $A_s$ | 253.15 | 500 | 1540 | 3 | 2 | 13 |
| $\varepsilon_{11} - \varepsilon_{12}$ | | 50 | 162 | 3 | 2 | 7 |
| | 285.15 | 500 | 1515 | 3 | 5 | 13 |
| | | 50 | 165 | 3 | 6 | 8 |
| Type $B_s$ | 253.15 | 500 | 1502 | 3 | 2 | 13 |
| $\varepsilon_{11} - \varepsilon_{12}$ | | 50 | 155 | 3 | 2 | 8 |
| | 285.15 | 500 | 1459 | 2 | 5 | 13 |
| | | 50 | 158 | 3 | 6 | 8 |
| Type $A_s$ | 253.15 | 500 | 500 | 1 | 2 | 10 |
| $\varepsilon_{12} - \varepsilon_{23}$ | | 50 | 50 | 1 | 2 | 6 |
| | 285.15 | 500 | 500 | 1 | 4 | 9 |
| | | 50 | 50 | 1 | 5 | 6 |

 

of the study, presented in this paper, evidence the following:

- The original model is able to reproduce the main behaviours of shape memory alloys.
- The original model describes the phase transformation through the tensor $\mathbf{X}$, work conjugate with the transformation strain, which results undetermined when $||\mathbf{e}^{\mathrm{tr}}||$ is zero.
- The numerical solution algorithm proposed by Souza *et al.* has some drawbacks. In particular, it is unclear how to start the Newton iteration for the solution of the non-linear system describing the material behaviour.
- Souza *et al.* do not address the construction of the tangent tensor, consistent with the time-discrete model.

These considerations stimulated us to work on the improvement of the model. In particular, at the actual state of the research the goals reached are:

- Model modification through the introduction of a new expression of the transformation stress $\mathbf{X}$ which results determined also in the elastic domain.
- Implementation of a modified algorithm that overcomes the problems highlighted for the original procedure.
- Development of the tangent matrix algorithmically consistent with the modified algorithm.
- Extensive numerical investigations showing the robustness and efficiency of the modified algorithm.

In conclusion, the original model, joined with the modified solution algorithm herein proposed, seems to be an effective tool to reproduce the stress-induced phase transformation and numerically simulate the behaviour of SMA components.

In the next feature the authors wish to introduce an unsymmetric law to catch the real SMA behaviour in tension and compression (along the line described in Appendix A.1), as well as to test the solution algorithm in the framework of a finite element code, simulating real cases of applications of SMA, in particular in biomedical engineering.

## APPENDIX A

### *A.1. Extension of the modified solution algorithm*

As already underlined, the original model is unable to catch the characteristic asymmetric behaviour of SMA during tension–compression test. To overcome this limit, a new type of limit function is introduced in the modified algorithm.

In particular, recalling that in SMA the hydrostatic pressure has a small influence on the martensitic transformation [13], we consider a Prager-type limit function depending on second and third scalar invariant of the deviatoric relative stress (respectively, $J_2$ and $J_3$):

$$F(\mathbf{X}) = F(J_2, J_3) = \sqrt{2J_2} + M\frac{J_3}{J_2} - R \tag{A1}$$

where

$$\begin{aligned} J_2 &= \tfrac{1}{2}\mathbf{X}^2 : \mathbf{1} \\ J_3 &= \tfrac{1}{3}\mathbf{X}^3 : \mathbf{1} \end{aligned} \tag{A2}$$

 

Indicated as $\sigma_t$ and $\sigma_c$ the critical transformation stresses (i.e. the stress values at which the transformation from parent to product phase starts in tension and compression, respectively), the identification of the parameters $M$ and $R$ with tension–compression test gives:

$$\begin{aligned} M &= 2\sqrt{\frac{2}{3}}\frac{\sigma_c\sigma_t}{\sigma_c+\sigma_t} \\ R &= \sqrt{\frac{27}{2}}\frac{\sigma_c-\sigma_t}{\sigma_c+\sigma_t} \end{aligned} \tag{A3}$$

The use of a new limit function do not change the state detection and the branch solution from a theoretical point of view, but cause some numerical modifications. In particular, to introduce the new expression of $F$ into the modified model we rewrite Equation (17) as follows:

$$\begin{cases} \mathbf{s} = 2G(\mathbf{e}-\mathbf{e}^{tr}) \\ \mathbf{X} = \mathbf{s} - [\tau_M(T) + h\|\mathbf{e}^{tr}\| + \gamma]\dfrac{\mathbf{e}^{tr}}{\|\mathbf{e}^{tr}\|} \\ \gamma \geqslant 0 \\ \mathbf{e}^{tr} = \mathbf{e}_n^{tr} + \Delta\zeta\dfrac{dF}{d\boldsymbol{\sigma}} \\ \|\mathbf{e}^{tr}\| \leqslant \varepsilon_L \\ F(\mathbf{X}) = \|\mathbf{X}\| + \dfrac{2MJ_3}{\|\mathbf{X}\|^2} - R \leqslant 0 \\ \Delta\zeta \geqslant 0 \quad \Delta\zeta F(\mathbf{X}) = 0 \end{cases} \tag{A4}$$

where

$$\frac{dF}{d\boldsymbol{\sigma}} = \frac{dF}{d\mathbf{X}} : \mathbb{I}_{dev} = \left[1 - \frac{4MJ_3}{\|\mathbf{X}\|^3}\right]\frac{\mathbf{X}}{\|\mathbf{X}\|} + 2M\left[\frac{\mathbf{X}}{\|\mathbf{X}\|}\right]^2 : \mathbb{I}_{dev} = \frac{dF}{d\hat{\mathbf{X}}}$$

The residual Equation (26) assumes the form:

$$\tilde{\mathbf{R}}^8(\mathbf{X},\Delta\zeta,\gamma) = \begin{cases} \mathbf{X} - \mathbf{s}^{TR} + 2G\Delta\zeta\dfrac{dF}{d\hat{\mathbf{X}}} + [\tau_M(T) + h\|\mathbf{e}^{tr}\| + \gamma]\dfrac{\mathbf{e}^{tr}}{\|\mathbf{e}^{tr}\|} = \mathbf{0} \\ \|\mathbf{X}\| + \dfrac{2MJ_3}{\|\mathbf{X}\|^2} - R = 0 \\ \|\mathbf{e}^{tr}\| - \varepsilon_L = 0 \end{cases} \tag{A5}$$

and similarly for Equation (25). The components of the Newton–Raphson tangent matrix change accordingly; in particular, for the CASE $PT_2$, we have:

$$\begin{aligned} \mathbf{R}_{,X}^{X} &= \mathbb{I} + (2G+h)\Delta\zeta\mathbb{F}^X + (\tau_M+\gamma)\Delta\zeta\mathbb{B}^e\,\mathbb{F}^X \\ \mathbf{R}_{,\Delta\zeta}^{X} &= (2G+h)\mathbf{F}^{\hat{X}} + (\tau_M+\gamma)\mathbb{B}^e : \mathbf{F}^{\hat{X}} \\ \mathbf{R}_{,\gamma}^{X} &= \mathbf{N}^e \\ \mathbf{R}_{,X}^{\Delta\zeta} &= \mathbf{F}^X \end{aligned}$$

 

$$
\begin{aligned}
R_{,\Delta\zeta}^{,\Delta\zeta} &= 0 \\
R_{,\gamma}^{,\Delta\zeta} &= 0 \\
\mathbf{R}_{,X}^{,\gamma} &= \Delta\zeta\mathbb{F}^X : \mathbf{N}^e \\
R_{,\Delta\zeta}^{,\gamma} &= \mathbf{N}^e : \mathbf{F}^{\hat{X}} \\
R_{,\gamma}^{,X} &= 0
\end{aligned}
$$

where

$$
\begin{aligned}
\mathbf{N}^X &= \frac{\mathbf{X}}{\|\mathbf{X}\|} \\
\mathbf{N}^e &= \frac{\mathbf{e}^{\mathrm{tr}}}{\|\mathbf{e}^{\mathrm{tr}}\|} \\
\mathbf{F}^X &= \frac{\mathrm{d}F}{\mathrm{d}\mathbf{X}} = \left[1 - \frac{4MJ_3}{\|\mathbf{X}\|^3}\right]\frac{\mathbf{X}}{\|\mathbf{X}\|} + 2M[\mathbf{N}^X]^2 \\
\mathbf{F}^{\hat{X}} &= \frac{\mathrm{d}F}{\mathrm{d}\hat{\mathbf{X}}} = \left[1 - \frac{4MJ_3}{\|\mathbf{X}\|^3}\right]\frac{\mathbf{X}}{\|\mathbf{X}\|} + 2M[\mathbf{N}^X]^2 - \frac{2}{3}M\mathbf{1} \\
\mathbb{B}^X &= \frac{1}{\|\mathbf{X}\|}[\mathbb{I} - \mathbf{N}^X \otimes \mathbf{N}^X] \\
\mathbb{B}^e &= \frac{1}{\|\mathbf{e}^{\mathrm{tr}}\|}[\mathbb{I} - \mathbf{N}^e \otimes \mathbf{N}^e] \\
\mathbb{F}^X &= \frac{\mathrm{d}}{\mathrm{d}\mathbf{X}}\left(\frac{\mathrm{d}F}{\mathrm{d}\hat{\mathbf{X}}}\right) = \frac{12MJ_3}{\|\mathbf{X}\|^4}[\mathbf{N}^X \otimes \mathbf{N}^X] - \frac{4M}{\|\mathbf{X}\|}[\mathbf{N}^X \otimes (\mathbf{N}^X)^2 + (\mathbf{N}^X)^2 \otimes \mathbf{N}^X] \\
&\quad + \left[1 - \frac{4MJ_3}{\|\mathbf{X}\|^3}\right]\mathbb{B}^X + \frac{2M}{\|\mathbf{X}\|}(\mathbf{1} \boxtimes \mathbf{N}^X + \mathbf{N}^X \boxtimes \mathbf{1})
\end{aligned}
$$

with the square tensor product $\boxtimes$ defined as $(\mathbf{A} \boxtimes \mathbf{B})\mathbf{C} = \mathbf{A}\mathbf{C}\mathbf{B}^{\mathrm{T}}$ according to the definition given by Del Piero [29].

Moreover, for the linearization of Equation (17d) we have:

$$
\begin{aligned}
\mathbf{e}_{,X}^{\mathrm{tr}} &= \Delta\zeta\mathbb{F}^X \\
\mathbf{e}_{,\Delta\zeta}^{\mathrm{tr}} &= \mathbf{F}^{\hat{X}} \\
\mathbf{e}_{,\gamma}^{\mathrm{tr}} &= \mathbf{0}
\end{aligned}
\tag{A6}
$$

The effect of the model extension is checked repeating the uni-axial tests described in Section 4.1. In particular, we consider the same material with $\sigma_{\mathrm{t}} = 43$ MPa and $\sigma_{\mathrm{c}} = 69$ MPa. In this way the ratio $\sigma_{\mathrm{t}}/\sigma_{\mathrm{c}}$ has a value ($\frac{2}{3}$) near to the SMA characteristic value [13] and, at the same time, $R$ remains equal to 45.

The asymmetric response of the material during tension–compression test is shown in Figure A1 (left part) for both the case pseudoelasticity and shape memory effect. An unexpected behaviour characterizes the torsion test results at 253.15 K (Figure A1 right part):

 

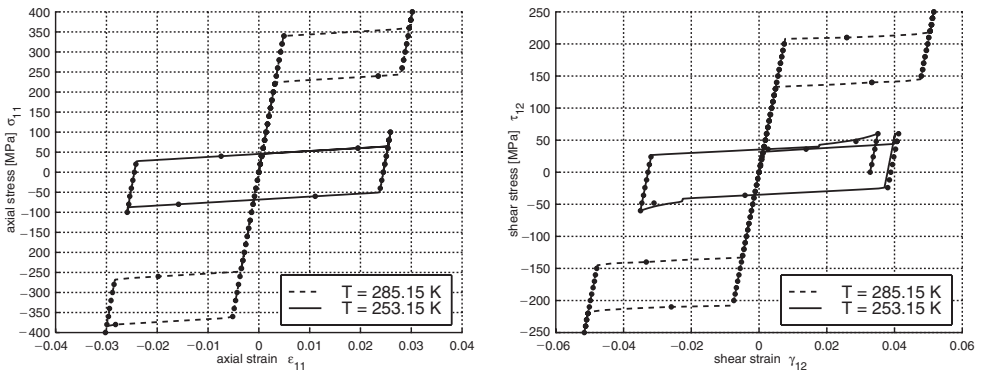


Figure A1. Extension of the modified algorithm. Tension-compression tests (left part): $T = 285.15$ K—integration time step 0.01 s (line) and 0.05 s (dot); $T = 253.15$ K—integration time step 0.01 s (line) and 0.2 s (dot). Torsion tests (right part): $T = 285.15$ K—integration time step 0.01 s (line) and 0.04 s (dot); $T = 253.15$ K—integration time step 0.01 s (line) and 0.2 s (dot).

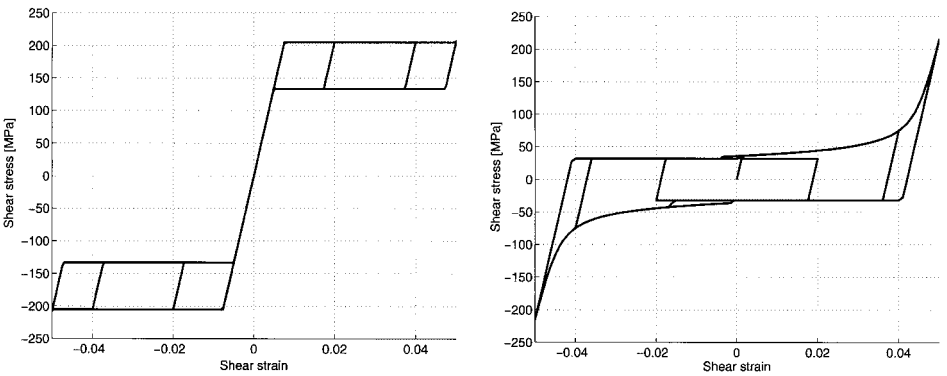


Figure A2. Extension of the modified algorithm. Cyclic torsion test at 2, 4 and 5% of deformation: $T = 285.15$ K (left part) $T = 253.15$ K (right part).

also if not fully explored, we believe that this is a consequence of the constraint condition on the transformation strain norm ($\|\mathbf{e}^{\mathrm{tr}}\| < \varepsilon_L$). Indeed, the model extension uses a $J2$-type norm to limit the transformation strain and a norm depending on both $J2$ and $J3$ to limit the transformation stress. Figure A2 shows cyclic torsion tests at different level of deformation (2, 4, 5%): it is evident how this kind of response affects only the martensitc phase.

ACKNOWLEDGEMENTS

The present work has been partially developed within the joint French-Italian 'Lagrange laboratory' project as well as partially supported by the Italian National Center of Research (C.N.R) through the 'Second Special Project for Advanced Technologies' ('Materiali Speciali per Tecnologie Avanzate II').

 

## REFERENCES


1. Funakubo H. *Shape Memory Alloys*. Gordon and Breach Science Publishers: London, 1987. Translated from the Japanese by J. B. Kennedy.
2. Fremond M. Shape memory alloys. A thermomechanical model. In *Free Boundary Problems*: *Theory and Applications*, Hoffmann KH, Sprekels J (eds). Vol. I. Longman Scientific & Technical: New York, 1990; 295–306.
3. Duerig TW, Melton KN, Stökel D, Wayman CM (eds). *Engineering Aspects of Shape Memory Alloys*. Butterworth-Heinemann: London, 1990.
4. Auricchio F, Sacco E. A temperature-driven beam for shape-memory alloys: constitutive modelling, finite-element implementation and numerical simulations. *Computer Methods in Applied Mechanics and Engineering* 1999; **174**:171–190.
5. Auricchio F. A robust integration-algorithm for a finite-strain shape memory-alloy superelastic model. *International Journal of Plasticity* 2001; **17**:971–990.
6. Liang C, Rogers CA. One-dimensional thermomechanical constitutive relations for shape memory materials. *Journal of Intelligent Materials Systems and Structures* 1990; **1**:207–234.
7. Graesser EJ, Cozzarelli FA. Shape memory alloys as new materials for aseismic isolation. *Journal of Engineering Mechanics* (ASCE) 1991; **117**:2590–2608.
8. Brinson LC. One-dimensional constitutive behavior of shape memory alloys: thermomechanical derivation with non-constant material functions and redefined martensite internal variables. *Journal of Intelligent Materials Systems and Structures* 1993; **4**:229–242.
9. Abeyaratne R, Kim SJ, Knowles JK. A one-dimensional continuum model for shape-memory alloys. *International Journal of Solids and Structures* 1994; **31**:2229–2249.
10. Liang C, Rogers CA. A multi-dimensional constitutive model for shape memory alloys. *Journal of Engineering Mathematics* 1992; **26**:429–443.
11. Graesser EJ, Cozzarelli FA. A proposed three-dimensional constitutive model for shape memory alloys. *Journal of Intelligent Materials Systems and Structures* 1994; **5**:78–89.
12. Patoor E, Eberhardt A, Berveiller M. Micromechanical modelling of the shape memory behavior. In *Mechanics of Phase Transformations and Shape Memory Alloys*. ASME: New York; 1994, 23–37.
13. Patoor E, Eberhardt A, Berveiller M. Micromechanical modelling of superelasticity in shape memory alloys. *Journal de Physique IV* 1995; **C8-5**:277–292.
14. Boyd JG, Lagoudas DC. A thermodynamical constitutive model for shape-memory materials. Part I. The monolithic shape-memory alloy. *International Journal of Plasticity* 1996; **12**:805–842.
15. Boyd JG, Lagoudas DC. A thermodynamical constitutive model for shape-memory materials. Part II. The SMA composite materials. *International Journal of Plasticity* 1996; **12**:843–873.
16. Leclercq S, Lexcellent C. A general macroscopic description of the thermomechanical behavior of shape memory alloys. *Journal of the Mechanics and Physics of Solids* 1996; **44**:953–980.
17. Souza AC, Mamiya EN, Zouain N. Three-dimensional model for solids undergoing stress-induced phase transformations. *European Journal of Mechanics—A/Solids* 1998; **17**:789–806.
18. Lemaitre J, Chaboche JL. *Mechanics of Solid Materials*. Cambridge University Press: Cambridge, 1990.
19. Lubliner J. *Plasticity Theory*. Macmillan: New York, 1990.
20. Liu Y, Xie Z, Van Humbeeck J, Delay L. Asymmetry of stress–strain curves under tension and compression for NiTi shape memory alloys. *Acta Materialia* 1998; **46**:4325–4338.
21. Orgéas L, Favier D. Stress-induced martensitic transformation of NiTi alloy in isothermal shear, tension and compression. *Acta Materialia* 1998; **46**:5579–5591.
22. Gall K, Sehitoglu H, Chumlyakov YI, Kireeva IV. Tension-compression asymmetry of the stress–strain response in aged single crystal and polycristalline NiTi. *Acta Materialia* 1999; **47**:1203–1217.
23. Liu Y, Van Humbeeck J. Damping capacity of shape memory alloy. In DSTN (ed.). *Memory Alloys for New Seismic Isolation and Energy Dissipation Device—Mainside Project*, Servizio Sismico Italiano, Rome, 1999; 59–72.
24. Crisfield MA. *Non-linear Finite Element Analysis of Solids and Structures*. Wiley: Chichester, 1996.
25. Simo JC, Hughes TJR. *Computational Inelasticity*. Springer-Verlag: Berlin, 1998.
26. Simo JC. Topics on the numerical analysis and simulation of plasticity. In Ciarlet PG, Lions JL (eds). *Handbook of Numerical Analysis*, Vol. III. Elsevier Science Publisher B.V.: Amsterdam, 1999.
27. Zienkiewicz OC, Taylor RL. *The Finite Element Method* (5th edn), Vol. II. Butterworth-Heinemann: New York, 2000.
28. Sittner P, Hara Y, Tokuda M. Experimental study on the thermoelastic martensitic transformation in shape memory alloy polycrystal induced by combined external forces. *Metallurgical and Materials Transactions* 1995; **26A**:2923–2935.
29. Del Piero G. Some properties of the set of fourth-order tensors with application to elasticity. *Journal of Elasticity* 1979; **3**:245–261.


 